Robotica: (2020) volume 38, pp. 1263–1287. © Cambridge University Press 2019
doi:10.1017/S0263574719001413

Gait Optimization for Quadruped Rovers

Lukas Zhornyak† and M. Reza Emami†‡*

† *Institute for Aerospace Studies, University of Toronto, Toronto, Canada, M3H 5T6*
E-mail: lukas.zhornyak@mail.utoronto.ca
‡ *Division of Space Engineering, Luleå University of Technology, Kiruna, Sweden, 98128*

(Accepted September 7, 2019. First published online: October 2, 2019)

SUMMARY
This paper studies the gait characteristics of a quadruped rover that mimics domestic cats, and attempts to optimize these characteristics. The kinematics and dynamics formulation of the rover's three-dimensional model is developed, and its gait, pose and corresponding control parameters are computed to minimize torque or maximize speed, using a genetic algorithm. The optimization model consists of a set of equality and inequality constraints that ensure the feasibility and stability of the gaits, while considering the entire gait spectrum that feline species exhibit. The optimal gaits for minimizing the torque closely resemble lateral sequence gaiting, with a trotting behaviour as speed increases. A running gait is obtained at the maximum speed. The optimization results appear to conform to the biological observations of feline species, suggesting the tendency of conserving energy in biological gaiting.

KEYWORDS: Quadruped rover; Gait planning; Gait optimization; Genetic algorithm.

1. Introduction

The study of legged locomotion is inspired by the locomotion capabilities of animals, which use different gaits at different speeds depending on factors such as energy consumption.[1] Despite extensive studies on animals locomotion (see ref. [2], as an example,) there are some key questions, still awaiting rigorous answers, about why animals adopt certain locomotion behaviours in various circumstances and whether their locomotion has converged to optimal gaits throughout their evolution. Theoretically, finding optimal gaits for a multi-legged system faces two major challenges: one is due to the complexity of kinematic and dynamic modelling of legged locomotion, and the other roots in developing proper optimization models and capable solution algorithms. The present work attempts to address both challenges for a quadruped rover model that mimics domestic cats.

In general, a comprehensive model of quadruped locomotion includes the three translational movements, that is, forward-backward thrust, upward-downward heave and sideways sway, as well as roll, yaw and pitch rotations. However, such models, albeit feasible, may end up computationally too complicated, and to some extent redundant, for optimization purposes. Thus, most works in the literature on gait optimization consider a two-dimensional (2D) model in the sagittal plane to study major aspects of quadruped locomotion, entirely avoiding the complexities of a three-dimensional (3D) model.[3] For example, a 2D rigid body model was used to simulate the locomotion of a horse from patterns of a given kinematic data set.[4] A fuzzy-logic-based control strategy was developed for creating simulated planar gallops in quadrupeds.[5] A 10-link planar simulation was used to test the feedforward and feedback strategies for controlling transverse gallops in a horse.[6] A kinematics-based simulation was developed in ref. [7] for studying articulated rovers traversing uneven terrains. In the present paper, the complete 3D simulation of a quadruped rover is utilized for gait optimizations; however, each optimization model is focused on the sagittal plane parameters, as the primary factors in quadruped locomotion, in order to guarantee the efficiency of the solution algorithm.

* Corresponding author. E-mail: emami@utias.utoronto.ca

https://doi.org/10.1017/S0263574719001413 Published online by Cambridge University Press

The locomotion of a quadruped rover is achievable by defining the trajectories of actuated joints.[8] Therefore, the goal of the gait optimization problem is to obtain optimal joint trajectories. Two approaches can be used for modelling such an optimization problem. In the first approach, the parameters defining the joint trajectories are directly optimized. This method has been used in various works, such as,[9] where joint trajectories are defined using polynomial functions. The second approach involves designing the motion of foot or toe of the legs, and obtaining the corresponding joint trajectories through the inverse kinematics model.[10] As a notable example, in ref. [11] the trajectory for the toes of a hexapod rover was selected as a cycloid during the swing phase (SW) and a uniform horizontal trajectory during stance phase (ST). The present paper uses the second approach, because it allows us to take into account some of the natural behaviours, for example, with respect to the leg impact at touchdown. Animals tend to retract their paws right before touchdown to reduce leg impact, and this has been shown to aid locomotion periodicity in legged rovers.[12,13] Further, continuous, periodic toe trajectories can be created, in this work by using a series of Bezier functions.

The gait optimization has been shown to be a non-linear, multi-constrained problem.[14] Many researchers have used evolutionary algorithms (EAs) to solve for the optimization problem, due to a number of reasons. First, EAs do not require a closed-form model,[15] which in case of quadruped rovers consists of highly coupled, non-linear relations. Secondly, EAs are known to be viable approaches when many design variables are involved with their interrelationships not necessarily known. The complexity and multi-dimensionality of the search space in problems such as gait optimization critically diminish the efficacy of standard gradient-search-based techniques.[16] Thirdly, EAs do not require continuity or differentiability of the associated objective function(s), and are capable of readily finding multiple local minima/maxima in the search space.[15] Lastly, with a suitable choice of population size, mutation and recombination rates in the EA, the algorithm can potentially become independent of the assigned initial population, hence showing strong global search capabilities. The gait optimization problem for a dog-like quadruped rover for various walking speeds is carried out in ref. [17]. An optimization of gaits for the Sony(R) AIBO(TM) robot is also carried out using genetic algorithms (GAs), as a form of EA, with the aid of AIBO hardware.[18–20] A biped humanoid robot for climbing slopes is suggested in ref. [21], and optimized using a GA to achieve maximum forward velocity and stability, as well as minimum energy consumption. The parameters of a hexapod rover are optimized using the GA for different locomotion speeds and periodic gaits.[11]

This paper develops an evolutionary optimization model to find near-optimal gaits for a cat-like quadruped rover, using a 3D simulation and considering the entire gait and pose variable spectrum. This differs from the works highlighted in the previous paragraph by both not constraining the gait to a specific sequence and not constraining the robot's movement to the sagittal plane, in effect attempting to find the optimal gait under the objective function with a minimum of constraints on the motion. The optimization model is based on defining smooth, continuous and periodic trajectories for the motion of the toe of each leg. Further, the results of minimum joint torque or maximum forward speed are evaluated by comparing them with those found in nature.

The remainder of the paper is organized into the following sections. Section 2 describes the quadruped rover model and the kinematics and dynamics formulations, while also detailing the Integrated Design and Simulation Environment (IDSE) developed for gait optimization. Section 3 defines the optimization variables, and discusses the objective functions, constraints and the GA used for the optimization. Section 4 provides the optimization results and their comparison with profiles observed in nature. Some concluding remarks are made in Section 5.

2. Quadruped Rover Model

An illustration of a quadruped rover and associated variables is given in Fig. 1. The main body B, with length L_B, mass M_B and inertia I_B, has no constraints on it motion in the world (inertial) frame {W}. The coordinates of the body centre of mass (O_B) in {W} are x_B, y_B and z_B. The pitch ψ_B angle describes the rotation of the body about y_B axis of the body frame B. Four bilaterally symmetric legs are attached to B, which collectively behave similarly to a parallel manipulator. The legs are labelled as FL (front left), FR (front right), HL (hind left) and HR (hind right). Each leg is modelled as a serial-link manipulator with three degrees of freedom, consisting of three links, of length L_1, L_2 and

https://doi.org/10.1017/S0263574719001413 Published online by Cambridge University Press

Table I. Body mass and geometric properties.

Length, L_B (cm)	**Width (cm)**	**Height (cm)**	**Mass M_B (kg)**
29.4	15.3	5.0	2.486

Table II. DH and mass parameters for the front and hind legs.

j	$a_j^{\mathrm{F}} = L_j^{\mathrm{F}}$ (cm)	α_j^{F}	d_j^{F} (cm)	m_j^{F} (kg)	$a_j^{\mathrm{H}} = L_j^{\mathrm{H}}$ (cm)	α_j^{H}	d_j^{H} (cm)	m_j^{H} (kg)
1	15.0	0	0	0.061	13.5	0	0	0.061
2	13.2	0	0	0.139	11.7	0	0	0.139
3	7.5	0	0	0.114	9.5	0	0	0.116

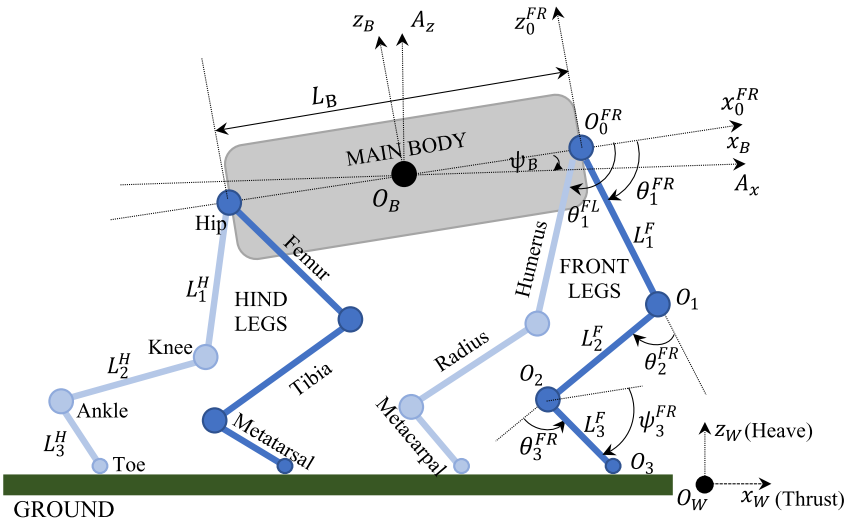


Fig. 1. Rover model in the sagittal plane.

L_3, connected with parallel revolute joints, the hip (O_0), knee (O_1) and ankle (O_2). The three joint angles in each leg are grouped as

$$q(t) = \left[\theta_1(t)\ \theta_2(t)\ \theta_3(t)\right] \tag{1}$$

where θ_i is the angle of link i with respect to the previous link (Fig. 1). For the front/hind legs, the links are called humerus/femur ($\overline{O_0O_1}$), radius/tibia ($\overline{O_1O_2}$) and metacarpal/metatarsal ($\overline{O_2O_3}$) links, respectively. The end point of metacarpal/metatarsal link, which touches the ground, is called the toe (O_3). The length of the links is selected proportionally to resemble that of a domestic cat without the phalanges.[22] The total leg length L_t is the sum of the length of the links. The physical parameters of the robot are summarized in Tables I and II.

The instant when the toe O_3 hits the ground is referred to as the leg's touchdown, where the rover is in its anterior extreme position (AEP) configuration. The instant when O_3 is lifted off the ground is referred to as the leg's take-off, where the rover is in its posterior extreme position (PEP) configuration. The leg movement from AEP to PEP is referred to as the SW, whereas the leg movement from PEP to AEP is referred to as the ST, as illustrated in Fig. 2.

2.1. Kinematics formulation

The locomotion of a quadruped rover can be considered as a sequence of cyclic motions, where each stride cycle is a period during which all four legs complete one SW and one ST. The successive stride cycles in quadruped animals are nearly identical,[23] so the body centre of mass O_{B} (Fig. 1) can be described as a distance λ (stride length) over time T (stride time) with a uniform horizontal speed

https://doi.org/10.1017/S0263574719001413 Published online by Cambridge University Press

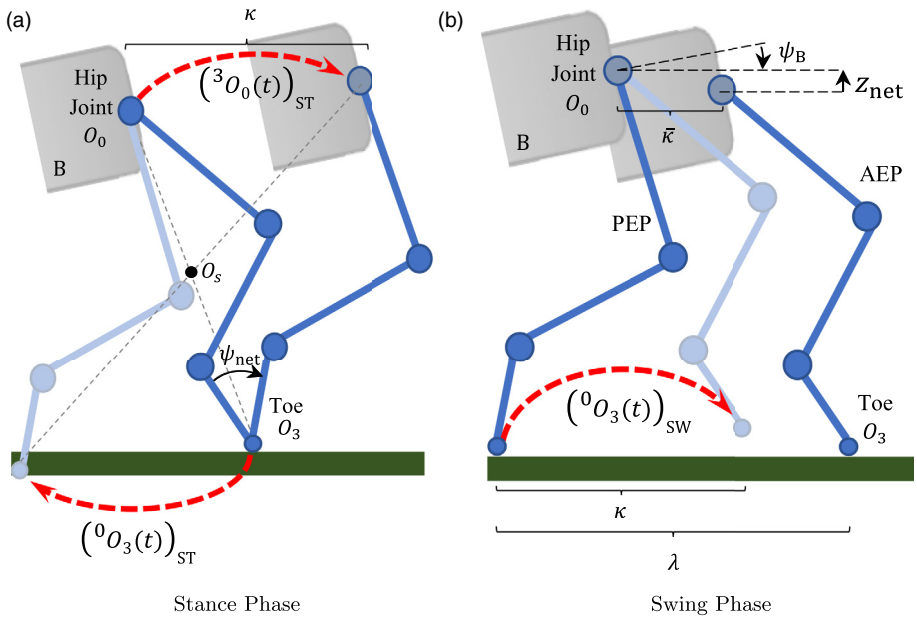


Fig. 2. Front leg models showing ST (a) and SW (b).

of $V_B = \lambda/T$. Two parameters are used to define the leg locomotion. The first one is the duty factor $\beta \in (0, 1)$ as the ratio of the duration of the ST to the stride time. Consequently, the duration of the ST and SW is βT and $(1 - \beta)T$, respectively. While most animals have a nearly identical duty factor across different legs, in this work independent duty factors are assumed for the legs for generality, namely β^{FL}, β^{FR}, β^{HL} and β^{HR}. The second parameter is the net distance $\bar{\kappa}$ travelled forward by the hip O_0 of each leg during its SW:

$$\bar{\kappa} = (1 - \beta)T * (\lambda/T) = (1 - \beta)\lambda \tag{2}$$

Since O_B moves λ meters ahead in one cycle, each hip joint must move the same distance forward in one cycle, as well. Hence, the distance κ that the leg's hip O_0 moves forward with respect to its toe O_3 during the ST can be defined as

$$\kappa = \lambda - \bar{\kappa} = \beta\lambda \tag{3}$$

To ensure that each leg returns to the same AEP after each cycle, the leg's toe O_3 must move forward horizontally with respect to its hip O_0 by κ during the SW. For this reason, κ is referred to as the step length (Fig. 2).

The rover motion can then be characterized by defining the relative phase $\phi \in (0, 1)$ as the offset in time between the touchdown of a leg to that of another arbitrarily reference leg, the FL leg in this work. Therefore, with the front left leg serving as a reference, three relative phase parameters, ϕ^{FR}, ϕ^{HL}, ϕ^{HR}, should be defined for other legs in general (Fig. 3a). As a special case, a symmetric gait refers to one in which the two legs of each leg group have a relative phase of 50% with respect to each other. In this case, a single phase parameter ϕ^{FH} can be used. Figures 3c–3e show three common symmetric gaits, namely pace, trot and the lateral sequence walk, respectively.

During the SW of each leg, the hip O_0 moves forward with body B along the trajectory $({}^WO_0(t))_{SW}$ expressed in {W} (where a pre-superscript signifies relation to the frame), while the toe O_3 moves along the trajectory $({}^0O_3(t))_{SW}$ expressed in frame {0}, which is the coordinate frame attached to the body at O_0 with x-axis along A_R. During the ST, the toe O_3 maintains contact with the ground. If no slippage occurs ($({}^WO_3(t))_{ST} = \text{const.}$), O_3 can be treated as a passive pivot about which O_0 follows the trajectory $({}^3O_0(t))_{ST}$. (Frame {3} is an inertial frame parallel to {W} with origin at O_3.) To avoid using {3} as a reference frame, $({}^0O_3(t))_{ST}$ can be used instead representing a rotation of π about O_S (Fig. 2).[24] As the toe O_3 moves backward along $({}^0O_3(t))_{ST}$, body B moves forward along $({}^3O_0(t))_{ST}$ as desired. Therefore, the desired motion of the rover can be translated into the desired toe trajectories $({}^0O_3(t))_{SW}$ and $({}^0O_3(t))_{ST}$ during SW and ST, respectively.

https://doi.org/10.1017/S0263574719001413 Published online by Cambridge University Press

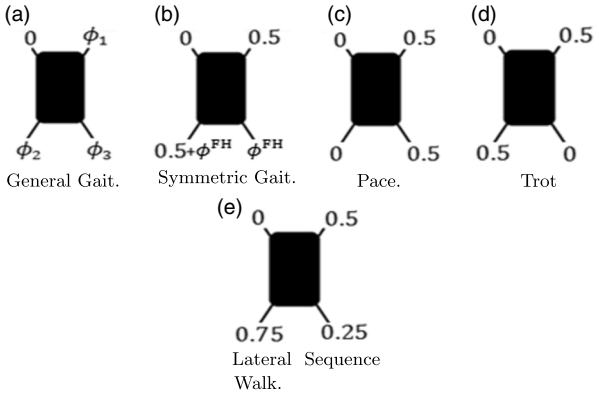


Fig. 3. The relative phases of the legs for a (a) general gait, (b) symmetric gait, (c) pace, (d) trot and (e) lateral sequence walk. Note that 0 is the reference leg.

The desired motion for each leg can be defined in each phase by using its toe position in the sagittal plane, $x_3(t)$ and $z_3(t)$, as well as the orientation of the metacarpal/metatarsal link $\psi_3(t)$, expressed in {0}, each in the form of a Bezier curve of order m:[25]

$$\delta_m(t) = \frac{1}{(t_f)^m} \sum_{k=0}^{m} \frac{m!}{k!(m-k)!} t^k (t_f - t)^{m-k} \cdot a_k \tag{4}$$

where t_f is the length of time taken for that phase. Bezier curves are chosen for this task, because they exhibit smooth curves and are insensitive to small perturbations in their coefficients. A Bezier curve of order m has $(m+1)$ coefficients a_k, requiring at least $(m+1)$ boundary conditions to solve for. Such boundary conditions are indeed the value of leg parameters (toe position and metacarpal/metatarsal link orientation) and their rate of change at the initial and phase transition times.

In this work, the AEP configuration at each cycle is considered to be the leg's initial configuration (see Section 3.2). This results in the initial leg parameters of ($x_{3,\mathrm{AEP}}$, $z_{3,\mathrm{AEP}}$, $\psi_{3,\mathrm{AEP}}$). Consequently, the corresponding parameters at PEP can be obtained from

$$x_{3,\mathrm{PEP}} = x_{3,AEP} - \beta\lambda \cos\psi_{\mathrm{B}} + z_{\mathrm{net}} \sin\psi_{\mathrm{B}} \tag{5}$$

$$z_{3,\mathrm{PEP}} = z_{3,\mathrm{AEP}} - \beta\lambda \sin\psi_{\mathrm{B}} + z_{\mathrm{net}} \cos\psi_{\mathrm{B}} \tag{6}$$

$$\psi_{3,\mathrm{PEP}} = \psi_{3,\mathrm{AEP}} - \psi_{\mathrm{net}} \tag{7}$$

where z_{net} is the net change in height of the hip in {W}, and ψ_{net} is the net change in orientation of the metatarsal/metacarpal link during ST/SW (Fig. 2).

Assuming that body B is travelling at a uniform velocity V_{B} horizontally with respect to {W}, while O_3 is stationary with respect to {W} during the ST, it is indeed moving with respect to {0} with magnitudes of $-V_{\mathrm{B}} \cos\psi_{\mathrm{B}}$ and $-V_{\mathrm{B}} \sin\psi_{\mathrm{B}}$ along x_0 and z_0, respectively. Hence,

$$\dot{x}_{3,\mathrm{PEP}} = -V_{\mathrm{B}} \cos\psi_{\mathrm{B}} \tag{8}$$

$$\dot{z}_{3,\mathrm{PEP}} = -V_{\mathrm{B}} \sin\psi_{\mathrm{B}} \tag{9}$$

Further, to eliminate impact effects caused by instantaneous changes in velocity, we assume

$$\dot{x}_{3,\mathrm{AEP}} = \dot{x}_{3,\mathrm{PEP}} \tag{10}$$

$$\dot{z}_{3,\mathrm{AEP}} = \dot{z}_{3,\mathrm{PEP}} \tag{11}$$

The $\dot{\psi}_3$ rates for AEP and PEP configurations are to be determined through the optimization problem, as it will be discussed in the next section (Section 3.2).

https://doi.org/10.1017/S0263574719001413 Published online by Cambridge University Press

By assuming that the maximum step clearance (f_c) occurs halfway between $x_{3,\mathrm{PEP}}$ and $x_{3,\mathrm{AEP}}$, one additional boundary condition is obtained for the SW:

$$(x_{3,\mathrm{m}}, z_{3,\mathrm{m}}) = \left(x_{3,\mathrm{PEP}} + \frac{\kappa}{2}\cos\psi_{\mathrm{B}} + f_c \sin\psi_{\mathrm{B}}, -\frac{\kappa}{2}\sin\psi_{\mathrm{B}} + f_c\cos\psi_{\mathrm{B}}\right) \tag{12}$$

Table AIV summarizes the boundary conditions and their derivations for each parameter/phase, as well as the order for the corresponding Bezier function. Using these boundary conditions, the proper coefficients a_k for the Bezier function (Eq. (4)) can be determined, thus obtaining the trajectories $({}^0O_3(t))_{\mathrm{SW}}$ and $({}^0O_3(t))_{\mathrm{ST}}$.

The motion of the quadruped rover is generated through the actuation of the three joints in each leg. Therefore, the above mentioned desired trajectories for the leg parameters should be related to the (desired) joint displacements in each leg through the following equations:

$$x_3 = L_1\cos(\theta_1) + L_2\cos(\theta_1+\theta_2) + L_3\cos(\theta_1+\theta_2+\theta_3) \tag{13}$$

$$z_3 = L_1\sin(\theta_1) + L_2\sin(\theta_1+\theta_2) + L_3\sin(\theta_1+\theta_2+\theta_3) \tag{14}$$

$$\psi_3 = \theta_1+\theta_2+\theta_3 \tag{15}$$

Equations (13)–(15) can be solved for the joint displacements analytically, and there exist two sets of joint angles (or leg configurations) for each desired set of (x_3, z_3, ψ_3). Therefore, to create a continuous profile for the joint displacements from the desired trajectories, the solution must increment in time starting from the initial joint angles $q(t=0) = q_0$ corresponding to the AEP configuration.

To begin the motion of the rover, the initial position of the body B centre of mass in the world frame must be defined. Assuming that at the start of the motion at least one leg is in ST (and all the other toes are on or above the ground), the initial vertical position can be defined as

$$\begin{aligned} {}^{\mathrm{W}}z_{\mathrm{B}} = \max\Bigg\{ & \left| x_3^{\mathrm{FL}}\sin(\psi_{\mathrm{B}}) + z_3^{\mathrm{FL}}\cos(\psi_{\mathrm{B}}) - \frac{L_{\mathrm{B}}}{2}\sin(\psi_{\mathrm{B}})\right|, \\ & \left| x_3^{\mathrm{FR}}\sin(\psi_{\mathrm{B}}) + z_3^{\mathrm{FR}}\cos(\psi_{\mathrm{B}}) - \frac{L_{\mathrm{B}}}{2}\sin(\psi_{\mathrm{B}})\right|, \\ & \left| x_3^{\mathrm{HL}}\sin(\psi_{\mathrm{B}}) + z_3^{\mathrm{HL}}\cos(\psi_{\mathrm{B}}) + \frac{L_{\mathrm{B}}}{2}\sin(\psi_{\mathrm{B}})\right|, \\ & \left| x_3^{\mathrm{HR}}\sin(\psi_{\mathrm{B}}) + z_3^{\mathrm{HR}}\cos(\psi_{\mathrm{B}}) + \frac{L_{\mathrm{B}}}{2}\sin(\psi_{\mathrm{B}})\right|\Bigg\}. \end{aligned} \tag{16}$$

where L_{B} is the distance between hind and front hips which is a rover parameter (Fig. 1), and ψ_{B} is the body pitch, which is an optimization variable. Further, the horizontal position of the body B centre of mass ${}^{\mathrm{W}}x_{\mathrm{B}}$ is initialized to zero.

Equations (4)–(16) are analytically solved and evaluated in MATLAB®, and this module is referred to as the Kinematics Trajectory Generator (KTG).

2.2. *Dynamics formulation*

The inverse dynamics (ID) of a fixed-base manipulator is well documented in the literature,[26] but the development of an ID formulation for moving-base manipulators, such as biped or quadruped rover, is an ongoing research. The dynamic equations for a six-wheeled rover are derived using Kane's method in ref. [27], but the work is not challenged by changing the contact points as in the case of legged rover. The dynamic equations for a six-legged, radially symmetric rover are derived using the Euler–Lagrange approach for a tripod, statically stable gait.[28] However, in our work the gait variables describe an entire range of gaits, which may not be statically stable. The approach developed in ref. [29] computes the ID torque in a reduced-dimensional null space of the constraints, using an orthogonal decomposition of the constraint Jacobian. Hence, contact forces need not be measured and used. Using this method in this paper, the rover's generalized coordinates are

$$\hat{q} = \left[q^{\mathrm{FL}}\ q^{\mathrm{FR}}\ q^{\mathrm{HL}}\ q^{\mathrm{HR}}\ r_{\mathrm{B}}\right]^T \in \mathbb{R}^{16} \tag{17}$$

https://doi.org/10.1017/S0263574719001413 Published online by Cambridge University Press

where $q \in \mathbb{R}^3$ represents the three joint angles for each of the four legs, and r_B represents the horizontal and vertical position of the body B centre of mass and its orientation, expressed in the world coordinate frame {W}:

$$r_{\mathrm{B}} = \left\{x_{\mathrm{B}}\ z_{\mathrm{B}}\ \psi_{\mathrm{B}}\ \theta_R\right\} \in \mathbb{R}^4 \tag{18}$$

The ID model can be formulated using the Euler–Lagrange equations:[26]

$$\hat{\tau} = M(\hat{q}) \cdot \ddot{\hat{q}} + C(\hat{q}, \dot{\hat{q}}) \cdot \dot{\hat{q}} + g(\hat{q}) - J_c(\hat{q})^T \cdot f \tag{19}$$

The generalized torque vector $\hat{\tau}$ in Eq. (19) is

$$\hat{\tau} = \left[\tau^{\mathrm{FL}}\ \tau^{\mathrm{FR}}\ \tau^{\mathrm{HL}}\ \tau^{\mathrm{HR}}\ 0\ 0\ 0\ 0\right]^T \in \mathbb{R}^{16} \tag{20}$$

where τ is the joint torque matrix for each of the four legs:

$$\tau = \left[\tau_1\ \tau_2\ \tau_3\right] \in \mathbb{R}^3 \tag{21}$$

The matrix $M \in \mathbb{R}^{16\times16}$ represents the inertia matrix, $C \in \mathbb{R}^{16\times16}$ is the matrix describing centrifugal and Coriolis effects and $g \in \mathbb{R}^{16}$ defines the gravitational field vector. The vector $f \in \mathbb{R}^8$ consists of the four horizontal F_x and four vertical F_z interaction forces between the ground and the toes:

$$f = \left[F_x^{\mathrm{FL}}\ F_x^{\mathrm{FR}}\ F_x^{\mathrm{HL}}\ F_x^{\mathrm{HR}}\ F_z^{\mathrm{FL}}\ F_z^{\mathrm{FR}}\ F_z^{\mathrm{HL}}\ F_z^{\mathrm{HR}}\right]^T \tag{22}$$

The constraint Jacobian $J_c \in \mathbb{R}^{8\times16}$ is defined as

$$J_c = \left[\frac{\partial \hat{p}}{\partial \hat{q}}\right]_{8\times16} \tag{23}$$

where

$$\hat{p} = \left[{}^{\mathrm{W}}x_3^{\mathrm{FL}}\ {}^{\mathrm{W}}x_3^{\mathrm{FR}}\ {}^{\mathrm{W}}x_3^{\mathrm{HL}}\ {}^{\mathrm{W}}x_3^{\mathrm{HR}}\ {}^{\mathrm{W}}z_3^{\mathrm{FL}}\ {}^{\mathrm{W}}z_3^{\mathrm{FR}}\ {}^{\mathrm{W}}z_3^{\mathrm{HL}}\ {}^{\mathrm{W}}z_3^{\mathrm{HR}}\right]^T \in \mathbb{R}^8 \tag{24}$$

and ${}^{\mathrm{W}}x_3$ and ${}^{\mathrm{W}}z_3$ are the horizontal and vertical position of the four toes in the world frame {W}. By carrying out a QR decomposition of the constraint Jacobian,[29] the unconstrained and constrained dynamics can be separated, and the joint torque τ can be can be solved.

The forward dynamics simulations (FDSs) of a quadruped rover can be performed through the following algorithm, using the subroutine INV $\left(\hat{q}, \dot{\hat{q}}, \ddot{\hat{q}}\right)$ for solving the rover's ID model as explained above:

Step 1: Having the initial values of $\hat{q}$ and $\dot{\hat{q}}$, solve the ID model for $\ddot{\hat{q}} = 0$:

$$\mathrm{INV}\left(\hat{q}, \dot{\hat{q}}, 0\right) = M(\hat{q}) \cdot 0 + C(\hat{q}, \dot{\hat{q}}) \cdot \dot{\hat{q}} + g\hat{q} - J_c(q)^T \cdot f$$

Step 2: LOOP $i = 1$ TO 16;

Put: $\ddot{\hat{q}} = \delta_i$, and solve: $M(\hat{q}) \cdot \delta_i = \mathrm{INV}(\hat{q}, \dot{\hat{q}}, \delta_i) - \mathrm{INV}(\hat{q}, \dot{\hat{q}}, 0)$
where δ_i is a 16×1 column matrix such that its ith element is unity and the rest is zero. Hence, in each loop, the column i of the inertia matrix M is calculated.

END

Step 3: By knowing M, $\hat{\tau}$ and $\mathrm{INV}(\hat{q}, \dot{\hat{q}}, 0)$, solve the following set of simultaneous equations for $\ddot{\hat{q}}$.

$$M(\hat{q}) \cdot \ddot{\hat{q}} = \hat{\tau} - \mathrm{INV}(\hat{q}, \dot{\hat{q}}, 0)$$

Step 4: Integrate $\ddot{\hat{q}}$ to obtain $\dot{\hat{q}}$ and then $\hat{q}$ for one step ahead in time, and continue steps $1 - 4$ for the next time increment.

2.3. Integrated design and simulation environment

The IDSE consists of the KTG and the FDS, and it was developed using MATLAB®/ Simulink® and their physical modelling toolboxes to compute the design attributes of the optimization problem,

https://doi.org/10.1017/S0263574719001413 Published online by Cambridge University Press

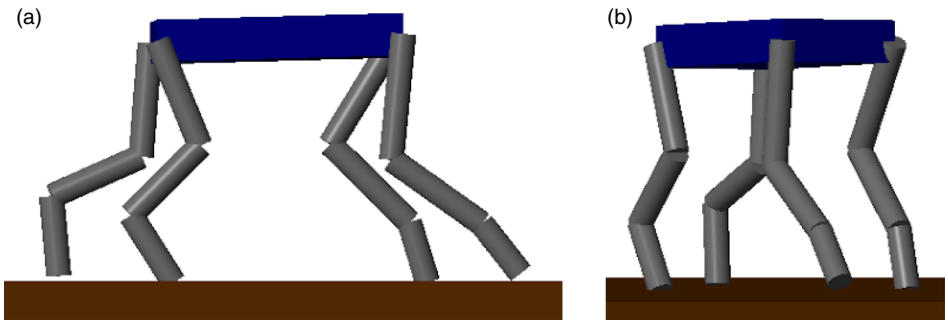


Fig. 4. Rover model built in Simulink®/SimMechanics®.

as it will be discussion in Section 3. Given a set of variables φ (Section 3.2) for any rover during the optimization process, the KTG creates the corresponding joint trajectories $q(t)$, as described in Section 2.1. Using φ and $q(t)$, the FDS is executed and the optimization attributes are calculated (Section 3). This iterative step is repeated for all rovers in a population, over multiple generations in the GA.

2.3.1. Rover model. As shown in Fig. 4, the rover model consists of a cuboidal main body and four legs. All parts are designed in accordance to the model outlined in the beginning of this section. The Denavit–Hartenberg (DH) parameters a, α and d[30] offer a convenient notation to represent the configuration of robot manipulators, and have been used in this work for the legs of the rover. The major advantage in using DH parameters is that the structure of the rover can be modified to resemble any other animal through a change in these parameters. The fourth DH parameter θ[31] corresponds to the joint angles q. The DH parameters selected for the rover (Table II), the mass of the entire rover (3.7 kg) and the length of the main body ($L_B = 0.29$ m) are based on data collected for domestic cats.[22] The links are designed as uniform cylindrical rods, with a density of aluminium (2700 kg/m^3), and link masses proportional to link lengths.

2.3.2. Environment model. The environment model consists of a standard gravity field and a spring-damper-based ground contact model.[32] The model uses a vertical position switch to apply appropriate forces to the toes. When the vertical position of the toe is greater than zero (no contact between the toe and the ground), no external force is applied to the toe. When there is contact, vertical reaction force (F_z) and horizontal frictional forces (F_x and F_y) are applied according to the following equations:[27]

$$F_z = k\varsigma^n + b\varsigma^p \dot{\varsigma}^q \tag{25}$$

$$\begin{aligned} F_x &= \mu_x F_z \\ F_y &= \mu_y F_z \end{aligned} \tag{26}$$

$$\begin{aligned} \dot{\mu}_x &= -3\left(\frac{|v_{t,x}|}{s_p}\right)\mu_x + 3\left(\frac{\mu_k}{s_p}\right)v_{t,x} \\ \dot{\mu}_y &= -3\left(\frac{|v_{t,y}|}{s_p}\right)\mu_y + 3\left(\frac{\mu_k}{s_p}\right)v_{t,y} \end{aligned} \tag{27}$$

where ς is the penetration distance of the toe into the surface, μ_x and μ_y are internal states of the friction model, $v_{t,x}$ and $v_{t,y}$ are the horizontal velocities of the toe measured with respect to the world frame {W} and μ_k is the coefficient of kinetic friction. The roles and values of the constants in these equations are summarized in Table III.

2.3.3. Verification and validation. Through the use of the physical modelling toolbox in Simulink®, it can be assumed that the calculations of the motion of the rover will be accurate. Along with the

https://doi.org/10.1017/S0263574719001413 Published online by Cambridge University Press

Table III. Descriptions and assigned values of constants used in friction model.

Constant	Description	Value
k	Spring constant of the ground	7.21×10^7
b	Damping constant of the ground	3.8×10^4
n, p, q	Exponential terms modelling non-linear effects	2.31, 1.1, 1
μ_k	Coefficient of kinetic friction	0.6
s_p	Displacement of toe before saturation of friction	1×10^{-3}

environment model presented in Section 2.3.2 and derived from ref. [32], this allows for straightforward verification of the model presented. Furthermore, the results presented in Section 4 appear to be reasonably similar to those of the feline on which the model is based, as discussed therein. This suggests that model is also valid.

3. Optimization Model

The optimization model of the quadruped rover consists of the objective functions, optimization variables, equality and inequality constraints, as well as the offline optimization algorithm, which will be discussed in this section.

3.1. Objective functions

3.1.1. Torque minimization. While some works have used different forms of the specific resistance, that is, the ratio of the maximum available power/energy to the maximum forward velocity travelled over a cycle,[33,34] this work selects a function that minimizes the average of total instantaneous joint torque τ over one stride cycle:[35]

$$\Gamma_{\mathrm{T}} = \frac{1}{T}\int_0^T \left(\|\tau^{\mathrm{FL}}\|^2 + \|\tau^{\mathrm{FR}}\|^2 + \|\tau^{\mathrm{HL}}\|^2 + \|\tau^{\mathrm{HR}}\|^2\right) dt \tag{28}$$

This provides an indication of the total load applied on the joints, and thus is proportional to the power consumption. This optimization is performed at four different speeds (0.10, 0.50, 1.00 and 1.50 m/s) as well as the one obtained from the speed maximization case.

3.1.2. Speed maximization. An alternative objective function that is considered in this study is the average of the horizontal speed of the body B centre of mass over one stride cycle. Although the horizontal speed of the body centre of mass is assumed to be constant (V_{B}) in this work, due to the numerical errors, it would be more accurate for the optimization to compute this objective function through the integration of the instantaneous horizontal speed of the centre of mass over the stride period:

$$\Gamma_{\mathrm{S}} = \frac{1}{T}\int_0^T (\dot{x}_{\mathrm{B}})\, dt \tag{29}$$

3.2. Optimization variables

To obtain an optimal motion of body B based on a certain objective function, such as joint torque or rover speed, the corresponding desired trajectories must be computed for the three joints in each leg (Eq. (1)). One approach to achieving the desired motion of the rover is to define $q(t)$ and derive the trajectories $({}^0O_3(t))_{\mathrm{SW}}$ and $({}^0O_3(t))_{\mathrm{SW}}$ using forward kinematics.[10] However, to allow for a better insight into the motion of the rover, the toe trajectories are instead defined first, and $q(t)$ is derived using inverse kinematics (as described in Section 2.1).

To obtain the appropriate boundary conditions for the Bezier functions (Eq. (4)) for the toe trajectories (Section 2.1), a number of parameters need to be defined as optimization variables, including

$$P_a^k = \left[\dot{\psi}_{\mathrm{AEP}}^k \;\; \dot{\psi}_{\mathrm{PEP}}^k \;\; \psi_{\mathrm{net}}^k \;\; z_{\mathrm{net}}^k \;\; f_c^k\right], \qquad k \in \{\mathrm{FL}, \mathrm{FR}, \mathrm{HL}, \mathrm{HR}\} \tag{30}$$

https://doi.org/10.1017/S0263574719001413 Published online by Cambridge University Press

where $\dot{\psi}^k_{\text{AEP}}$ and $\dot{\psi}^k_{\text{PEP}}$ are the angular velocities at AEP and PEP, ψ^k_{net} is the net change in the angular position of metacarpal/metatarsal link from PEP to AEP, z_{net} is the net change in the vertical position of the hip joint from PEP to AEP and f^k_c is the maximum step clearance during the SW. Further, computing $q(t)$ for each leg using inverse kinematics requires the initial position of the leg, for which either AEP or PEP can be used; the former option is selected in this work. Consequently, the initial position of the legs must also be included in the optimization variables:

$$P^k_b = q^k_0 = \left[\theta_{1}{}^k_{\text{AEP}}\ \theta_{2}{}^k_{\text{AEP}}\ \theta_{3}{}^k_{\text{AEP}}\right], \qquad k \in \{\text{FL, FR, HL, HR}\} \tag{31}$$

Finally, the stride length, body pitch and initial y velocity also need to be defined as optimization variables:

$$P_c = \left[\lambda\ \psi_{\text{B}}\ \dot{y}_{\text{B},i}\right] \tag{32}$$

The set of P^k_a, P^k_b and P_c is referred to as the Pose (P) optimization variables.

Additional parameters must be defined as optimization variable to describe the gait of the rover, including the duty factor β and relative phases ϕ of the legs, referred to as Gait (G) optimization variables:

$$G = \left[\beta^{\text{FL}}\ \beta^{\text{FR}}\ \beta^{\text{HL}}\ \beta^{\text{HR}}\ \phi^{\text{FR}}\ \phi^{\text{HL}}\ \phi^{\text{HR}}\right] \tag{33}$$

Furthermore, to ensure that each joint follows a desired trajectory, its movement should be controlled. Servo controllers have been successfully used for quadruped rovers,[36] which is adopted in this work. To find the optimal values of control gains, in this case proportional (K_P) and derivative (K_D), for each of the three joints ($K_{P,j}$, $K_{D,j}$, $j = 0, 1, 2$) of the front and hind legs during each phase of a cycle, they are also included in the optimization model as the Control (K) optimization variables:

$$\begin{gathered} K^k = \left[(K_{P,j})^k_{\text{SW}}\ (K_{D,j})^k_{\text{SW}}\ (K_{P,j})^k_{\text{ST}}\ (K_{D,j})^k_{\text{ST}}\right] \\ j = 0, 1, 2, \qquad k \in \{\text{FL, FR, HL, HR}\} \end{gathered} \tag{34}$$

The Pose, Gait and Control optimization variables form the set φ_{T} for the torque minimization:

$$\varphi_{\text{T}} = [P^{\text{FL}}_a\ P^{\text{FL}}_b\ P^{\text{FR}}_a\ P^{\text{FR}}_b\ P^{\text{HL}}_a\ P^{\text{HL}}_b\ P^{\text{HR}}_a\ P^{\text{HR}}_b\ P_c\ G\ K^{\text{FL}}\ K^{\text{FR}}\ K^{\text{HL}}\ K^{\text{HR}}] \in \mathbb{R}^{89} \tag{35}$$

For the speed maximization, to compute for the objective function (Eq. (29)), the stride time (T) should also be included in the optimization variables, resulting in the φ_{S} optimization variable set:

$$\varphi_{\text{S}} = [P^{\text{FL}}_a\ P^{\text{FL}}_b\ P^{\text{FR}}_a\ P^{\text{FR}}_b\ P^{\text{HL}}_a\ P^{\text{HL}}_b\ P^{\text{HR}}_a\ P^{\text{HR}}_b\ P_c\ G\ K^{\text{FL}}\ K^{\text{FR}}\ K^{\text{HL}}\ K^{\text{HR}}\ T] \in \mathbb{R}^{90} \tag{36}$$

The φ_{T} and φ_{S} optimization variable sets are summarized in Table AV.

3.3. Constraints

3.3.1. Phase boundary constraints. As the leg transitions between ST and SW, sudden changes occur in the degrees of freedom and their derivatives. This can result in physical impacts on the system causing energy dissipation. Without restoring energy into the system, it cannot repeat its periodic motion. Hence, to ensure smooth and continuous movement between the SW and ST to sustain a periodic motion, the following constraints are imposed on the joint angles q of each leg:

$$q_{\text{ST},i} = q_{\text{SW},f} = q_0 \tag{37}$$

$$q_{\text{SW},i} = q_{\text{ST},f} \tag{38}$$

$$\dot{q}_{\text{ST},i} = \dot{q}_{\text{SW},f} \tag{39}$$

$$\dot{q}_{\text{SW},i} = \dot{q}_{\text{ST},f} \tag{40}$$

where i and f subscripts denote the initial and final states of the joint angles, respectively.

3.3.2. Touchdown constraints. Animals tend to retract their legs prior to touchdown, a behaviour that has been shown to help with motion periodicity.[12,13] This can be mimicked in the rover model by reducing the absolute velocity of the toe at touchdown to eliminate impact effects:

https://doi.org/10.1017/S0263574719001413 Published online by Cambridge University Press

$$(v_{t,x})_{SW,f} = (v_{t,y})_{SW,f} = (v_{t,z})_{SW,f} = 0 \tag{41}$$

3.3.3. Contact constraints. By definition, during the SW, the toe O_3 must not contact the ground, whereas during the ST, the toe O_3 must remain in contact with the ground.

$$\left({}^{W}z_3(t)\right)_{SW} > 0 \tag{42}$$

$$\left({}^{W}z_3(t)\right)_{ST} = 0 \tag{43}$$

Further, to prevent slippage the friction force should be sufficiently large, so that there is no horizontal movement at the toe during the ST:

$$\left(v_{t,x}(t)\right)_{ST} = \left(v_{t,y}(t)\right)_{ST} = 0 \tag{44}$$

In addition, the initial value of the horizontal position of the toe in the world frame is also set equal to its value at the end of the SW. This way the robot begins its stance at the same point where it touched down.

$$\left({}^{W}x_3\right)_{ST,i} = \left({}^{W}x_3\right)_{SW,f} \tag{45}$$

Also, the toe's vertical position at the start as well as the end of the SW must be zero:

$$\left({}^{W}z_3\right)_{SW,i} = \left({}^{W}z_3\right)_{SW,f} = 0 \tag{46}$$

3.3.4. Maximum torque constraints. The maximum torque available for each joint is limited to

$$|\tau| < \tau_{max} = \left[\tau_{1,max}\ \ \tau_{2,max}\ \ \tau_{3,max}\right] \tag{47}$$

3.3.5. Gait stability. In the quadruped legged locomotion, the stability of a gait can be realized using criteria such as zero moment point,[35] eigenvalues of the Poincaré map, change of angular momentum and the ground reference points.[37] This work adopts the definition of stability presented in ref. [38]. It defines the *basin of fall* as a "subset of the state space that leads to a fall, (where) a point on the rover, other than a point on the foot (toe in this case), touches the ground." A periodic gait is stable then if and only if the rover is never in the basin of fall. Together, the phase boundary and numerical computation constraints will ensure that the rover does not fall during each period.

3.3.6. Numerical computation constraints. For certain optimization variable sets φ, the solver in Simulink® may not converge to any solution, or the solution may be unrealistic or impractical. To avoid such circumstances, the model computation is terminated and discarded if any of the following constraints are violated:

$$q(t) \text{ exists and can be found with the KTG} \tag{48}$$

$$\Delta t \geq \Delta t_{min} \tag{49}$$

$${}^{W}\dot{x}_B = V_B \tag{50}$$

$$z_B > 0 \tag{51}$$

$$|\psi_B| \leq \psi_{B,max} \tag{52}$$

$${}^{W}z_3^k \leq {}^{W}z_0^k, \qquad k \in \{FL, FR, HL, HR\} \tag{53}$$

where Δt is the required time increment for solving the simulation. The individual roles of these equations are summarized as follows:

- Equation (48) ensures that the desired toe positions are physically realizable.
- Equation (49) ensures that the produced motion is numerically stable.

https://doi.org/10.1017/S0263574719001413 Published online by Cambridge University Press

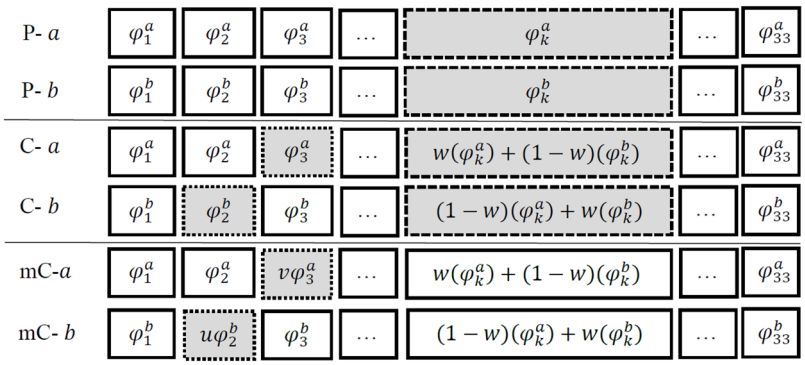


Fig. 5. Recombination and mutation – Parents P-a and P-b undergo arithmetic recombination to give children C-a and C-b, which undergo mutation to give mutated children mC-a and mC-b.

- Equation (50) ensures that the actual horizontal velocity of the body matches the expected velocity, ensuring that the overall motion is linear and uniform.
- Equation (51) ensures that body does not contact the ground, and hence ensures the gait is stable (see Section 3.3.5).
- Equation (53) ensures that the toe is never above the hip during the gait.

3.4. Optimization algorithm

The minimum torque and maximum speed optimizations are carried out using a GA,[31,39] which has been studied and used extensively for optimizing legged rovers.[11,17–21] An initial population of n rovers is created, where each rover has a randomly generated φ_T or φ_S. After evaluating all members in the population, they are ranked based on the value of their objective function (Section 3.1). From this population, two members are randomly picked up, and the member with the better rank is selected as a parent (binary tournament selection). Repeating this process n times generates the parent pool. These parents undergo arithmetic recombination in pairs to generate n children, which in turn are mutated (Fig. 5) and then evaluated. The best n rovers from the combined children and parent pools are selected to represent the new population. Details on various recombination and recombination and mutation techniques used in GAs can be found in.[31,39] This iterative process is repeated numerous times, until convergence is reached. Convergence is defined here as the first population where the difference between the average value of the objective function for the best 50%, 20% and 10% of the population is less than 1% of their combined average value.

A random initial population was used as the input for each optimization procedure. In the specific case of torque minimization at maximum velocity, the best member of the final generation of speed optimization was randomly permuted in all dimensions to form the initial population of the torque optimization, as discussed in Section 4.1.1. Optimization stops when the convergence criterion described previously is met.

The population size, recombination rate and mutation rate should be selected carefully to prevent a premature convergence to a local solution. If n is too small, the population may experience genetic drift and converge prematurely. If n is too large, on the other hand, the required simulation time may be exceedingly large. This work selects $n = 100$ as a trade-off. A suitable recombination and mutation rate can also help diversify the population at each generation, thereby reducing chances of premature convergence. This rate determines what percentage of variables are affected during each step. The fractional rate for recombination and mutation is selected as 30% and 10%, respectively.

On the machine used for this paper (Intel® Core™ i7 with 16GB memory), each generation of 100 rovers took approximately 2 min to evaluate.

4. Results and Discussion

The optimization process described in Section 3 was applied to the robot model described in Section 2. In the first part of this section, the results of the maximum speed optimization are discussed and compared with the results of a subsequent minimum torque optimization performed at the same speed. The second part of this section examines select trends in the results of the minimum

https://doi.org/10.1017/S0263574719001413 Published online by Cambridge University Press

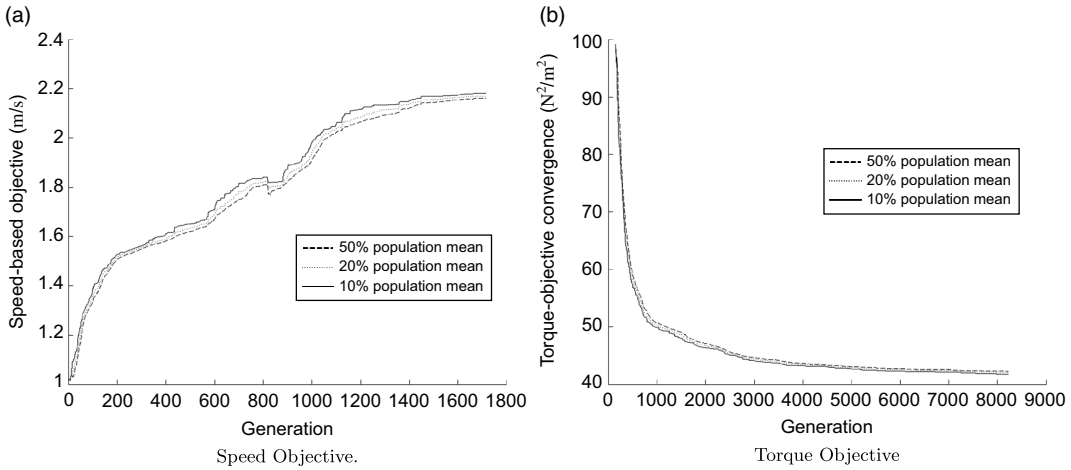


Fig. 6. Convergence of objective functions versus the number of generations elapsed.

torque optimization at increasing speeds. The optimal design variables obtained are listed in Tables AVI, AVII, AVIII, AIX, AX, AXI.

4.1. Behaviour at maximum obtained speed

4.1.1. Objective convergence. The convergence of the speed objective function in the speed maximization problem is shown in Fig. 6a. The speed maximization converged to a maximum speed of 2.17 m/s. This speed differs from the theoretical values derived solely from $V_B = \lambda/T = 1.97$ m/s and using λ and T that were also obtained from the speed optimization, as opposed to simulated results. The difference can be due to the fact that some of the constraints, including touchdown constraints (Eq. (41)), were defined with some margins to help the optimization arrive at feasible solutions. While an ideal solution is expected to adhere to all constraints as defined, some small margin of deviation from these constraints was required to account for the numerical nature of the simulations. This would allow the toe to slip slightly at touchdown, resulting in increasing the overall speed of the rover. Since such effect is merely due to the optimization model, the theoretical maximum speed was used along with the other optimum variables as a seed for the torque optimization. Theoretically, slippage is not accounted for in the rover model, so any slippage observed in the simulation can be expected to produce some deviation from the expected movement. Deviations in the movement result in increased corrective torque; therefore, the optimal minimum torque solution should have little to no slippage. The convergence of the torque optimization at the maximum speed is shown in Fig. 6b. In both optimizations, the three curves, depicting the average value of the objective function for the best 50%, 20% and 10% of the population, all approach a steady value of maximum speed or minimum total joint torque, respectively.

Figures 6a and 6b also show that the torque objective took longer to converge than the speed objective, requiring more than four times the number of generations. This may be because the value of the speed objective is only directly dependent on the stride length and stride time. Therefore, as long as the gaiting remains stable, improvements in the speed objective can be obtained through the random mutation of only these variables. In comparison, the value of torque objective is likely dependent on many more of the parameters, thus requiring a more gradual changes in the parameter values.

The torque minimization converged to a minimum total torque of 43.39 Nm, which is ∼3.3 times smaller than the value of the total torque required in the speed maximization, that is, 143.0 Nm.

4.1.2. Joint angle trajectories. Figure 7 shows the difference in the configuration of the rover at the front left leg's AEP and PEP for the two gaits produced by the speed maximization and torque minimization problems. At a cursory glance, the two configurations appear to be similar. This is to be expected since the gait produced by the speed maximization was used as a seed for the torque minimization. On closer inspection, the larger stride length (0.564 vs. 0.436 m) produced by the torque minimization, the difference in relative phases and the steeper body pitch (−2.69° vs. −0.92°) are clearly visible.

https://doi.org/10.1017/S0263574719001413 Published online by Cambridge University Press

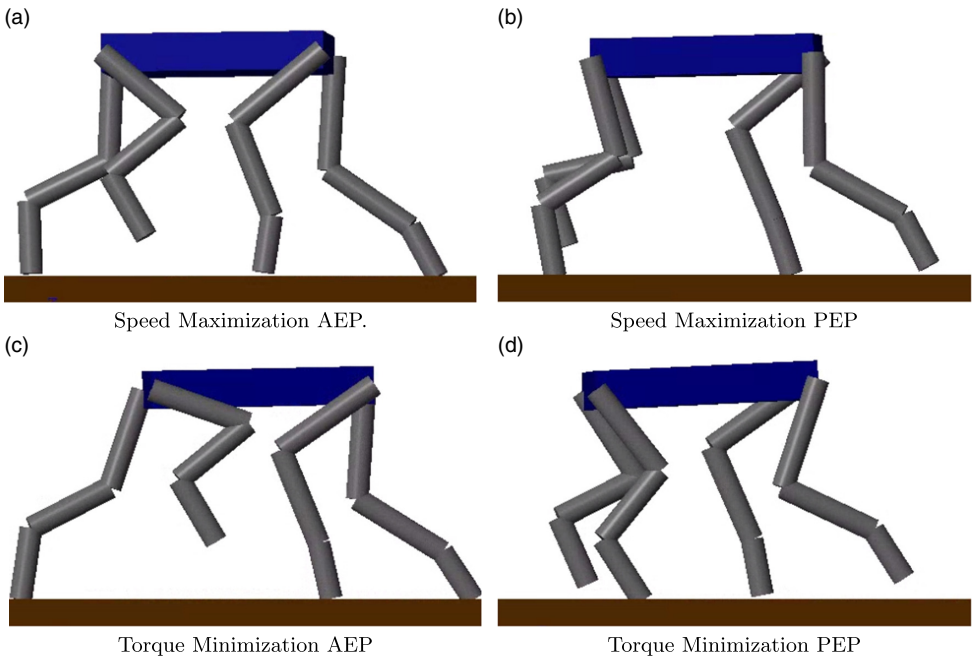


Fig. 7. Visualization of gaits at the AEP and PEP of the front left leg.

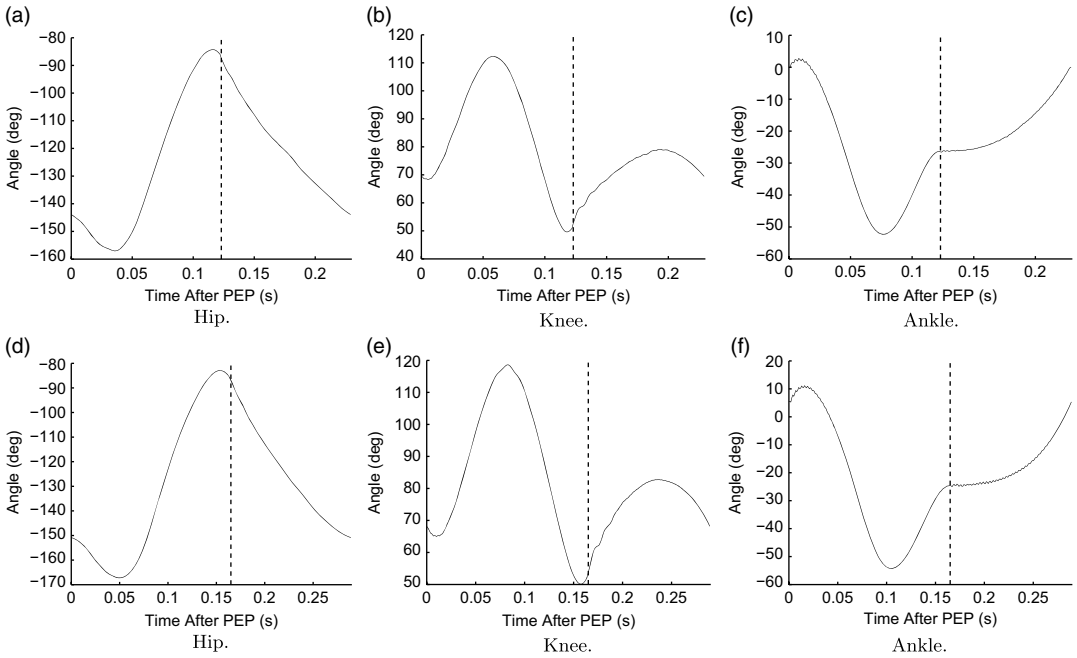


Fig. 8. Joint trajectories for the front left leg during one cycle at a nominal speed of 1.97 m/s. (a)–(c) speed maximization and (d)–(f) torque minimization.

Considering the front left leg only, the similarity between the two gaits remains in their angular trajectories (Fig. 8) and angular velocities (Fig. 9). The figures begin at the take-off of the leg and show one complete cycle; touchdown is shown by a dashed line. While β seems approximately the same for the leg in both gaits, this does not hold for the other legs. Nevertheless, the same general pattern in the trajectory continues to hold.

In the SW, the front left leg follows a retraction-extension pattern as seen in the change in sign of the angular velocity of each joint midway through the SW. This pattern breaks the contact with the ground, and creates the desired step clearance f_c. The hip joint is the first to change direction, ending

https://doi.org/10.1017/S0263574719001413 Published online by Cambridge University Press

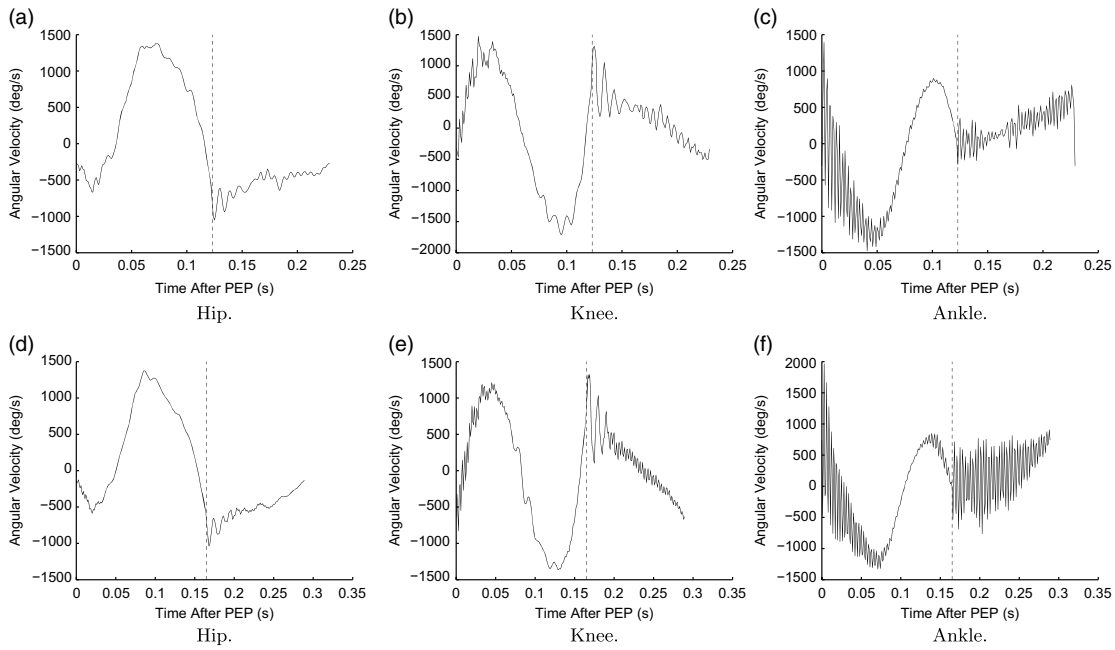


Fig. 9. Angular speeds for the front left leg during one cycle at a nominal speed of 1.97 m/s. (a)–(c) speed maximization and (d)–(f) torque minimization.

the SW with a further forward position than at take-off, and driving the leg forward to its AEP configuration. As the leg approaches touchdown, the angular velocity of each joint rapidly decreases to its respective initial velocities during ST, reducing impact effects and resulting in a continuous transition in the joint angles between SW and ST.

In the ST, the hip angle decreases at an approximately uniform speed, driving the leg backward, and thus the rover forward. The knee and ankle follow a similar retraction-extension pattern to that experienced during SW, albeit with a much smaller magnitude. This ensures that the toe maintains a uniform horizontal velocity through the ST.

The only major difference between the angular trajectories of the optimizations is a small increase in the amplitude of the movement, which is a result of the increase in stride length. The pattern described here is actually a general pattern, observed at every other speed with minor variation caused by differences in β and λ. This pattern can also be observed in the results obtained from natural feline gaits.[40,41]

4.1.3. Gait and torque. Figure 10 illustrates the torque applied at each joint of the front left leg during one cycle, beginning at the PEP of the front left leg. The AEP of the front left leg is marked by a dashed line while the AEPs and PEPs of the other three legs are marked by dotted line. Together, these lines denote instantaneous changes in the support of the rover corresponding to the gait, with the spaces in between labelled A through H. For the result produced by speed maximization, the order of these events is

FL PEP – FR AEP – HL AEP – HR PEP – FL AEP – FR PEP – HR AEP – HL PEP – FL PEP

producing a sequence primarily comprised of double-support (B, D, F, H) periods with brief triple-support (C, E, G) and single-support (A) periods. For the result obtained from torque minimization, the order varies only slightly

FL PEP – FR AEP – HL AEP – HR PEP – FR PEP – FL AEP – HL PEP – HR AEP – FL PEP

but produces a sequence primarily comprised of double-support (B, D, F, H) and single-support (A, E, G) periods, with a brief triple-support (C) period.

The most noticeable difference between the results of the two optimizations is the large increase in the amount of time spent in the single-support period after torque minimization. As opposed to

https://doi.org/10.1017/S0263574719001413 Published online by Cambridge University Press

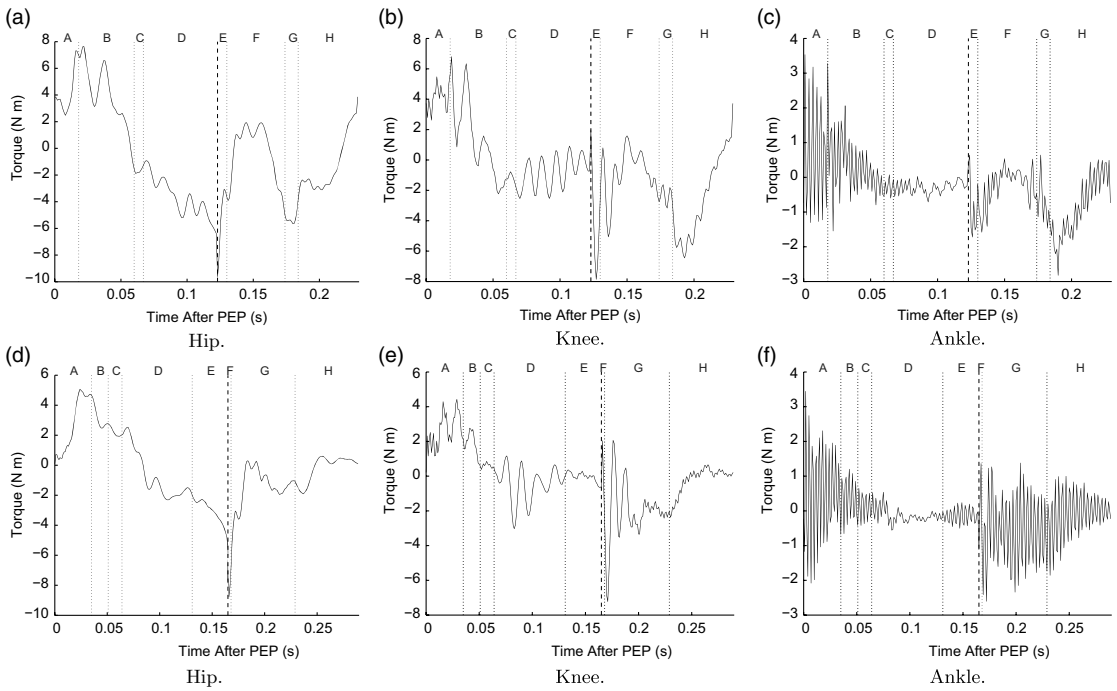


Fig. 10. Torque applied at actuated joints in the front left leg during one cycle at a nominal speed of 1.97 m/s. The top set of figures show the result produced through speed maximization while the bottom set shows the result produced through torque minimization.

being almost entirely comprised of double-support periods in speed maximization, the time spent in double-support and single-support is nearly equal in torque minimization. Additionally, while the result produced from speed optimization is nearly symmetric and is very close to a lateral sequence gait, the result of torque minimization is closer to a trotting gait than a lateral sequence gait.

The difference in gaits as well as the increase in stride length in torque minimization can explain the reduction of overall joint torque. During much of the swing cycle in both optimizations, the torque exerted by the knee and ankle joints hovers around zero. By increasing the stride length, the stride time and thus the duration of the SW increases. This means that the knee and ankle joints spend longer time hovering around zero torque, because most of the work needed to accelerate and decelerate the angular rotation of the joints can be done by gravity acting on the links. For the same reason, the hip torque is also reduced in the torque minimization gait. Further, during the ST a large spike in the applied torque for all three joints in and after sub-phase G is seen in speed maximization gait, corresponding to the switching support in the hind legs between left and right sides. The drastic change in the support of the rover requires a large torque to accommodate. Comparatively, there is no such drastic change in support during the ST of torque minimization gait. Interestingly, the impact of touchdown is about the same in both gaits.

The lateral sequence gait of speed maximization is more typical of a walking gait, while the trot of torque minimization is the gait that would be expected in a cat moving at 1.97 m/s.[40,42,43]

The oscillations of the joint torque (and the consequent oscillations in the joint speed shown in Fig. 9) are the by-product of the dynamics of the servo controllers at the joints, rather than indicative of the desired motion. In particular, the optimal solutions for the proportional gains result in high values, which in turn cause such fluctuations in the control torque. Nevertheless, the overall motion remains mostly free from these oscillations, as seen in Fig. 8. The greater oscillations at the knee and ankle are expected as these joints operate on less mass.

4.2. Some trends at increasing speeds

Torque minimization was also performed at slower speeds. Trials were conducted at 0.1, 0.5, 1.0 and 1.5 m/s. Despite being seeded with the results of the speed maximization, the result of the trial at maximum speed (1.97 m/s) conform with those at slower speeds. Some of the notable observations are highlighted in the following.

https://doi.org/10.1017/S0263574719001413 Published online by Cambridge University Press

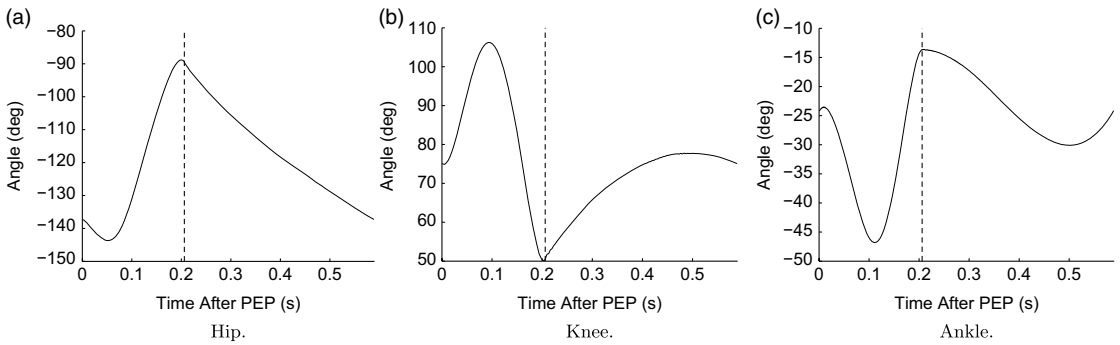


Fig. 11. Joint trajectories for the front left leg during one cycle, beginning at the take-off, at a nominal speed of 0.50 m/s. Touchdown is shown by a dashed line.

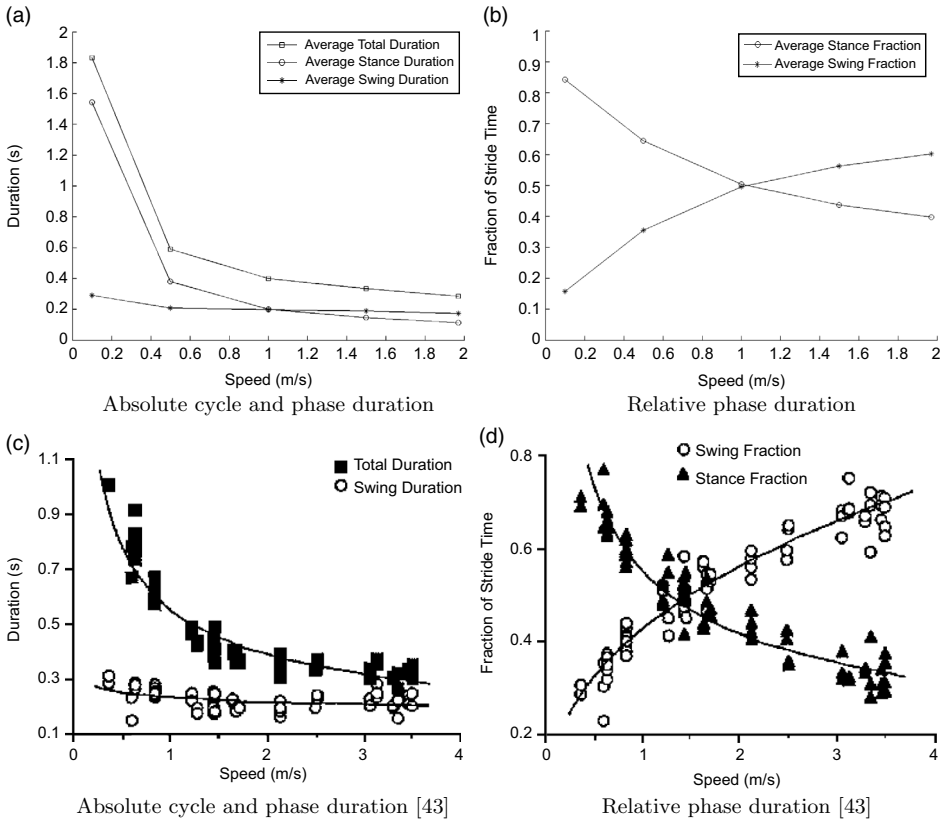


Fig. 12. Absolute and relative phase duration versus speed.

4.2.1. Joint angle trajectories. Figure 11 shows the angular trajectories of the gait produced by torque minimization at 0.50 m/s. The general pattern at this lower speed is consistent with the pattern observed in Fig. 8. However, the proportion of ST to SW is larger at a lower speed, visible in the scaling of the different sections. A shorter stride length is also visible in the smaller amplitude of pattern oscillation. The only other significant difference between the patterns in Figs. 8 and 11 is that at the (low) speed of 0.50 m/s, the angle of the ankle at touchdown is larger than the angle at take-off, whereas at the maximum speed, it is the other way around.

4.2.2. Phase duration. The absolute cycle and phase duration is shown in Fig. 12a, while the duration of the SW and ST as a fraction of the cycle duration is shown in Fig. 12b. Some biological observations for domestic cats are shown in Figs. 12c and 12d.[43] Similar observations are also reported in.[40] At low speeds, a cycle is primarily in ST. As the speed increases, the duration of the ST decreases while the duration of the SW remains relatively constant. At higher speeds, the SW occupies the majority of the cycle duration.

https://doi.org/10.1017/S0263574719001413 Published online by Cambridge University Press

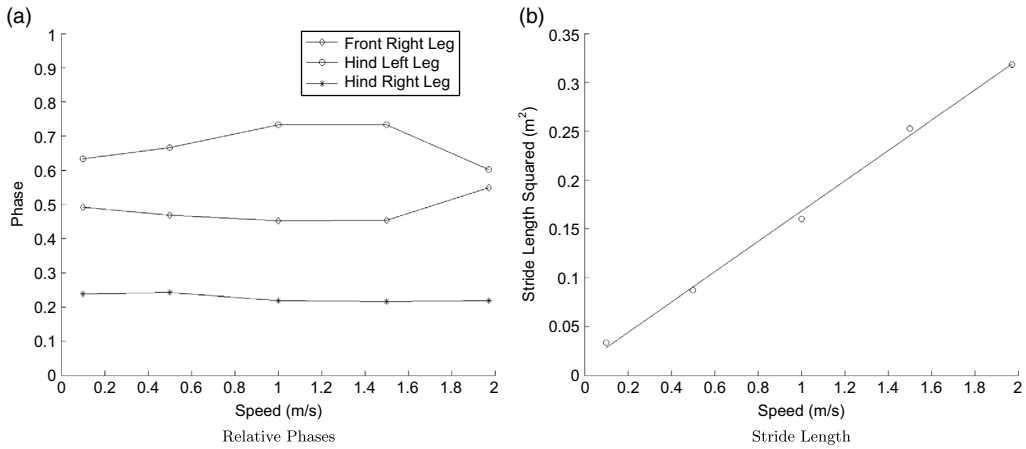


Fig. 13. Trend in the gait *G* optimization variables with increasing speed. Line of best fit obtained for the stride length with adjusted $R^2 = 0.973$.

The results obtained from the simulation appear to conform to the biological observations of feline species. There is some disparity at higher speeds, however, in a sense that the speed at the point where the duration of the ST and SW are equal is slightly slower in the simulation than in real life. This inconsistency may simply be the result of the mobility limitations in the developed rover model. Nevertheless, the torque optimization results clearly show that feline species likely optimize their energy (effort) in their gaiting.

4.2.3. Gait parameters. Figure 13a shows the phase of the legs relative to the front left leg versus the horizontal speed of the rover. The rover exhibits a gait most similar to a lateral sequence gait at each of the trials. However, at the maximum speed, the front right and hind left legs have relative phases more similar to a trotting gait. As discussed in refs.,[40,42,43] this is around the speed in which feline species also begin transitioning to a trot.

Figure 13b shows the trend in the square of the stride length versus the horizontal speed of the rover. A very strong linear relationship is observed in this graph, with an adjusted R^2 of 0.994. Since the speed of the rover is equal to stride length over the stride time, this would suggest a linear relationship between the reciprocal of the square root of stride time and speed. As can be seen in Fig. 12a, this is indeed the case.

From Figs. 12a and 12b, it can be inferred that as the speed increases there is a transition from gaits being primarily comprised of triple-support periods to those with double-support periods.

Finally, at the maximum speed periods were observed in the simulation, where both of the front legs or both of the hind legs were in the SW at the same time, which is a characteristic of running gaits.

4.2.4. Torque objective. Figure 14a demonstrates a linear trend in the square root of the torque objective with increasing speed. As described in Section 3.1, the torque objective represents the average of the sum of the squared instantaneous joint torque across a cycle. The square root of this quantity is then an indicator of the average magnitude of the instantaneous torque being exerted by all the joints.

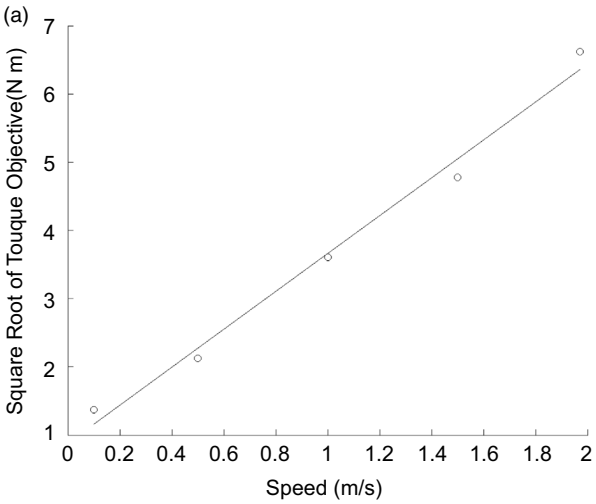
In domestic cats, a linear relationship is observed between speed and oxygen consumption, as a measure of the average power being exerted by the animal, as demonstrated in Fig. 14b.[44] Since the minimum torque obtained from the optimizations increases linearly with respect to speed (Fig. 14a), the power increases quadratically. This suggests that the model used in the optimizations is unable to recover the utilized energy as efficiently as a domestic cat is able to.

5. Conclusion

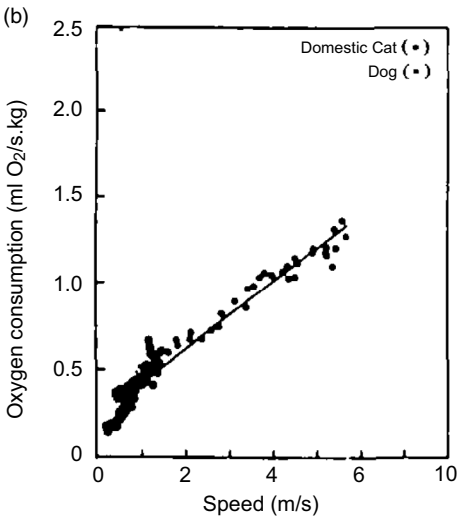
In this work, a 3D model of a quadruped rover, based on a domestic cat, was developed to optimize its gait, pose and control parameters. The multi-constraint optimization problem was solved, using a GA, to minimize the total joint torque or maximize the rover's speed.

The optimal gait was found to be similar to a lateral sequence at all speeds and to follow a consistent profile for each joint. With increasing speed, the optimal gait showed some of the characteristics of a trotting gait. At the maximum speed (1.97 m/s), a double SW in either the front or hind legs

https://doi.org/10.1017/S0263574719001413 Published online by Cambridge University Press



Trend in the minimum torque with increasing speed. Line of best fit obtained with an adjusted $R^2 = 0.977$.



Oxygen consumption (ml O_2/s · kg) versus speed (m/s) [44].

Fig. 14. Trend in the minimum torque and energy consumption of the simulated model and living cats, respectively, with increasing speed.

signified a running gait. With increasing speed, the stride lengths of the optimal solutions increased, the duty factors as well as duration of the ST decreased, while duration of the SW remained relatively constant. These results are consistent with those found in nature, suggesting that torque (power) conservation is one of the factors contributing to the evolution of the gaiting patterns in feline species.

Future works can further explore methods of controlling the sagittal behaviour, which was a source of instability in the simulations. Mimicking the ability of recovering energy in natural muscles (by replacing the last joint with a spring, as one example) may also reduce the torque required for the desired gaits. Performing similar optimizations for models based on other animal species may yield meaningful insights into biological locomotion behaviours.

References

1. J. Usherwood, "Why not walk faster?" *Biol. Lett.* **1**(3), 338–341 (2005).
2. M. Silva and J. Machado, "A historical perspective of legged robots," *J. Vib. Control* **13**(9–10), 1447–1486 (2007).
3. S. Coros, A. Karpathy, B. Jones, L. Reveret and M. Panne, "Locomotion skills for simulated quadrupeds," *ACM Trans. Graph.* **30**(4), 59:1–59:11 (2011).
4. A. Bogert, H. Schamhardt and A. Crowe, "Simulation of quadrupedal locomotion using a rigid dynamics model," *J. Biomech.* **22**(1), 33–41 (1989).

https://doi.org/10.1017/S0263574719001413 Published online by Cambridge University Press

5. D. Marhefka, D. Orin, J. Schmiedeler and K. Waldron, "Intelligent control of quadruped gallops," *IEEE/ASME Trans. Mech.* **8**(4), 446–456 (2003).
6. H. Herr and M. McMohan, "A galloping horse model," *Int. J. Robot. Res.* **20**(1), 26–37 (2001).
7. M. Tarokh and H. D. Ho, "Kinematics-based simulation and animation of articulated rovers traversing uneven terrains," *Robotica* **37**(6), 1057–1072 (2019).
8. A. N. Sarmah, A. Boruah, D. Kalita, D. Neog and S. Paul, "A bio-inspired implementation of walking and stair climbing on a quadruped robot," *Procedia Comput. Sci.* **143**, 671–677 (2018).
9. J. Vermeulen, D. Lefeber and B. Verrelst, "Control of foot placement, forward velocity and body orientation of a one-legged hopping robot," *Robotica* **21**(1), 45–57 (2003).
10. R. Paul, *Robot Manipulators: Mathematics, Programming, and Control: the Computer Control of Robot Manipulators*, Artificial Intelligence Series (MIT Press, Cambridge, 1981).
11. M. Silva, R. Barbosa and T. Machado, "Ga Optimization of an Hexapod Robot Parameters for Periodic Gaits," **In:** *Proceedings of 1st International Symposium on Computational Intelligence for Engineering Systems*, Porto, Portugal (2009).
12. A. Seyfarth, H. Geyer and H. Herr, "Swing-leg retraction: A simple control model for stable running," *J. Exp. Biol.* **206**, 2547–2555 (2003).
13. M. Wisse, C. Atkeson and D. Kloimwieder, "Swing Leg Retraction Helps Biped Walking Stability," **In:** *Proceedings of 5th IEEE-RAS International Conference on Humanoid Robots*, Tsukuba, Japan (2005), pp. 295–300.
14. L. Hu and C. Zhou, "Eda-Based Optimization and Learning Methods for Biped Gait Generation," *Robotic Welding, Intelligence and Automation* (T.-J. Tarn, S.-B. Chen and C. Zhou, eds.), vol. 362 (2007) pp. 541–549.
15. G. Daoxiong, J. Yan and G. Zuo, "A review of gait optimization based on evolutionary computation," *Appl. Comput. Intell. Soft Comput.* **2010** (2010).
16. M. Shrivastava, A. Dutta and A. Saxena, "Trajectory generation using ga for an 8 dof biped robot with deformation at the sole of the foot," *J. Intell. Robot. Syst. Theo. Appl.* **49**(1), 67–84 (2006).
17. K. Kiguchi, Y. Kusumoto, K. Watanabe, K. Izumi and T. Fukuda, "Energy-optimal gait analysis of quadruped robots," *Artif Life Robot.* **6**(3), 120–125 (2002).
18. S. Chernova and M. Veloso, "An Evolutionary Approach to Gait Learning for Four-Legged Robots," **In:** *Proceedings of the IEEE/RSJ International Conference on Intelligent Robots and Systems*, Sendai, Japan, vol. 3 (2004) pp. 2562–2567.
19. G. Hornby, M. Fujita, S. Takamura, T. Yamamoto and O. Hanagata, "Autonomous Evolution of Gaits with the Sony Quadruped Robot," **In:** *Proceedings of the Genetic and Evolutionary Computation Conference*, Orlando, Florida (1999) pp. 1297–1304.
20. M. Kim and W. Uther, "Automatic Gait Optimisation for Quadruped Robots," **In:** *Australasian Conference on Robotics and Automation*, Brisbane, Australia (2003).
21. S. Bi, Z. Zhuang, T. Xia, H.-X. Mo, H.-Q. Min and R.-H. Luo, "Multi-Objective Optimization for a Humanoid Robot Walking on Slopes," **In:** *Proceedings of IEEE Conference on Machine Learning and Cybernetics*, Guilin, China (2011) pp. 1261–1267.
22. L. Day and B. Jayne, "Interspecific scaling of the morphology and posture of the limbs during locomotion of cats (felidae)," *J. Exp. Biol.* **210**, 642–654 (2007).
23. R. Alexander, "The gaits of bipedal and quadrupedal animals," *Int. J. Robot. Res.* **3**(2), 49–59 (1984).
24. K. Tsujita, K. Tsuchiya and A. Onat, "Locomotion Control of a Multipod Locomotion Robot with CPG Principles," **In:** *Proceedings of the 6th International Symposium of Artificial Life and Robotics*, vol. 2 (2001) pp. 421–426.
25. E. Westervelt, J. Grizzle, C. Chevallereau, J. Choi and B. Morris, *Feedback Control of Dynamic Bipedal Robot Locomotion*, Automation and Control Engineering (CRC Press, New York, 2007).
26. J. J. Craig, *Introduction to Robotics: Mechanics and Control*, Addison-Wesley Series in Electrical and Computer Engineering: Control Engineering. (Pearson, Prentice Hall, 2005).
27. A. Meghdari, R. Karimi, H. Pishkenari, A. Gaskarimahalle and S. Mahboobi, "An effective approach for dynamic analysis of rovers," *Robotica* **23**(6), 771–780 (2005).
28. Z. Wang, X. Ding, A. Rovetta and A. Giusti, "Mobility analysis of the typical gait of a radial symmetrical six-legged robot," *Mechatronics* **21**(7), 1133–1146 (2011).
29. M. Kalakrishnan, "Learning, planning, and control for quadruped locomotion over challenging terrain," *Int. J. Robot. Res.* **30**(2), 236–258 (2011).
30. J. Denavit and R. Hartenberg, "A kinematic notation for lower-pair mechanisms based on matrices," *Trans ASME J. Appl. Mech.* **22**, 215–221 (1955).
31. A. Konak, D. Coit and A. Smith, "Multi-objective optimization using genetic algorithms: A tutorial," *Reliab. Eng. Syst. Saf.* **91**(9), 992–1007 (2006).
32. D. Wight, "A foot placement strategy for robust bipedal gait control," *Ph.D. Thesis*, (University of Waterloo, Canada, 2008).
33. T. Kang, H. Kim, T. Son and H. Choi, "Design of Quadruped Walking and Climbing Robot," **In:** *Proceedings of IEEE Conference on Intelligent Robots and Systems*, Las Vegas, NV (2003) pp. 619– 624.
34. E. Briskin, V. Chernyshev and A. Maloletov, "On Conception of Walking Machines Designing," **In:** *Proceedings of IEEE Conference on Advanced Robotics*, Coimbra, Portugal (2003) pp. 1763–1768.
35. M. Silva and J. Machado, "Kinematic and dynamic performance analysis of artificial legged systems," *Robotica* **26**(1), 19–39 (2008).

https://doi.org/10.1017/S0263574719001413 Published online by Cambridge University Press

36. C. Maufroy, H. Kimura and K. Takase, "Integration of posture and rhythmic motion controls in quadrupedal dynamic walking using phase modulations based on leg loading/unloading," *Auton. Robots* **28**(3), 331–353 (2010).
37. P. Roan, A. Burmeister, A. Rahimi and K. Holz, "Real-World Validation of Three Tipover Algorithms for Mobile Robots," **In:** *IEEE International Conference on Robotics and Automation*, Anchorage, Alaska (2010) pp. 4431– 4436.
38. J. Pratt and R. Tedrake, "Velocity-Based Stability Margins for Fast Bipedal Walking," **In:** *Fast Motions in Biomechanics and Robotics: Optimization and Feedback Control* (Springer, Berlin, Heidelberg, 2007).
39. H. Tamaki, H. Kita and S. Kobayashi, "Multi-Objective Optimizations by Genetic Algorithms: A Review," **In:** *Proceedings of IEEE International Conference on Evolutionary Computation*, Nagoya, Japan (1996) pp. 517–522.
40. G. E. Goslow, R. M. Reinking and D. G. Stuart, "The cat step cycle: Hind limb joint angles and muscle lengths during unrestrained locomotion," *J. Morphol.* **141**(1), 1–41 (1973).
41. J. Smith, S. Chung and R. Zernicke, "Gait-related motor patterns and hindlimb kinetics for the cat trot and gallop," *Exp. Brain Res.* **94**(2), 308–322 (1993).
42. D. Wisleder, R. Zernicke and J. Smith, "Speed-related changes in hindlimb intersegmental dynamics during the swing phase of cat locomotion," *Exp. Brain Res.* **79**(3), 651–660 (1990).
43. J. A. Vilensky and M. C. Patrick, "Inter and intratrial variation in cat locomotor behavior," *Physiol. Behav.* **33**(5), 733–743 (1984).
44. C. Taylor, N. Heglund and G. Maloiy, "Energetics and mechanics of terrestrial locomotion," *Exp. Biol.* **97**(1–2) (1982).

Appendix A

Table AIV. Boundary conditions and order for the Bezier functions.

Trajectory	Boundary Condition	Variable	Relation to optimization variables	Bezier function order
$x(t)_{ST}$	$x\|_{t=0}$	x_{AEP}	From θ_{AEP}, Eq. (13)	4
	$x\|_{t=t_{ST}}$	x_{PEP}	From θ_{AEP}, λ, β, Eqs. (3), (5) and (13)	
	$\frac{dx}{dt}\|_{t=0}$	$\dot{x}_{AEP}$	From V_B, ψ_B, Eq. (8)	
	$\frac{dx}{dt}\|_{t=t_{ST}}$	$\dot{x}_{PEP}$	From V_B, ψ_B, Eq. (10)	
$x(t)_{SW}$	$x\|_{t=t_{ST}}$	x_{PEP}	Described above	4
	$x\|_{t=t_{ST}+t_{SW}}$	x_{AEP}	Described above	
	$\frac{dx}{dt}\|_{t=t_{ST}}$	$\dot{x}_{PEP}$	Described above	
	$\frac{dx}{dt}\|_{t=t_{ST}+t_{SW}}$	$\dot{x}_{AEP}$	Described above	
$z(t)_{ST}$	$z\|_{t=0}$	z_{AEP}	From θ_{AEP}, Eq. (14)	4
	$z\|_{t=t_{ST}}$	z_{PEP}	From θ_{AEP}, λ, β, Eqs. (3), (6) and (14)	
	$\frac{dz}{dt}\|_{t=0}$	$\dot{z}_{AEP}$	From V_B, ψ_B, Eq. (9)	
	$\frac{dz}{dt}\|_{t=t_{ST}}$	$\dot{z}_{PEP}$	From V_B, ψ_B, Eq. (11)	
$z(t)_{SW}$	$z\|_{t=t_{ST}}$	z_{PEP}	Described above	5
	$z\|_{t=t_{ST}+t_{SW}}$	z_{AEP}	Described above	
	$\frac{dz}{dt}\|_{t=t_{ST}}$	$\dot{z}_{PEP}$	Described above	
	$\frac{dz}{dt}\|_{t=t_{ST}+t_{SW}}$	$\dot{z}_{AEP}$	Described above	
	$z\|_{t=t_{ST}+\frac{t_{SW}}{2}}$	z_m	From θ_{AEP}, f_c Eqs. (12) and (14)	
$\psi(t)_{ST}$	$\psi\|_{t=0}$	ψ_{AEP}	From θ_{AEP}, Eq. (15)	4
	$\psi\|_{t=t_{ST}}$	ψ_{PEP}	From θ_{AEP}, ψ_{net} Eqs. (7) and (15)	
	$\frac{d\psi}{dt}\|_{t=0}$	$\dot{\psi}_{AEP}$	$\dot{\psi}_{AEP}$	
	$\frac{d\psi}{dt}\|_{t=t_{ST}}$	$\dot{\psi}_{PEP}$	$\dot{\psi}_{PEP}$	
$\psi(t)_{SW}$	$\psi\|_{t=t_{ST}}$	ψ_{PEP}	Described above	4
	$\psi\|_{t=t_{ST}+t_{SW}}$	ψ_{AEP}	Described above	
	$\frac{d\psi}{dt}\|_{t=t_{ST}}$	$\dot{\psi}_{PEP}$	Described above	
	$\frac{d\psi}{dt}\|_{t=t_{ST}+t_{SW}}$	$\dot{\psi}_{AEP}$	Described above	

https://doi.org/10.1017/S0263574719001413 Published online by Cambridge University Press

Table AV. The pose, gait and control variables for leg k, $k \in$ FL,FR,HL,HR.

φ	Variables	Notes	**Total: 90 (ϕ_T)** **91 (ϕ_S)**
P_a^k	$\theta^k_{1\,\mathrm{AEP}}$	Hip joint angle at AEP for leg k	4
	$\theta^k_{2\,\mathrm{AEP}}$	Knee joint angle at AEP for leg k	4
	$\theta^k_{3\,\mathrm{AEP}}$	Ankle joint angle at AEP for leg k	4
P_b^k	$\dot{\psi}^k_{\mathrm{AEP}}$	Metacarpal/Metatarsal's angular velocity at AEP for leg k	4
	$\dot{\psi}^k_{\mathrm{PEP}}$	Metacarpal/Metatarsal's angular velocity at PEP for leg k	4
	ψ^k_{net}	Metacarpal/Metatarsal's net angular change for leg k	4
	z^k_{net}	Net change in hip's height during stance for leg k	4
	f^k_c	Toe's step clearance during SW for leg k	4
P_c	λ	Stride length	1
	ψ_{B}	Body Pitch	1
	$\dot{y}_{\mathrm{B},i}$	Initial out of sagittal plane velocity	1
G	β^k	Duty factor for leg k	4
	ϕ^k	Relative phase for leg k, $k \neq$ FL	3
K^k	$K^k_{\mathrm{P},1\mathrm{SW}}$	Proportional gain for hip joint during swing for leg k	4
	$K^k_{\mathrm{D},1\mathrm{SW}}$	Derivative gain for hip joint during swing for leg k	4
	$K^k_{\mathrm{P},1\mathrm{ST}}$	Proportional gain for hip joint during stance for leg k	4
	$K^k_{\mathrm{D},1\mathrm{ST}}$	Derivative gain for hip joint during stance for leg k	4
	$K^k_{\mathrm{P},2\mathrm{SW}}$	Proportional gain for knee joint during swing for leg k	4
	$K^k_{\mathrm{D},2\mathrm{SW}}$	Derivative gain for knee joint during swing for leg k	4
	$K^k_{\mathrm{P},2\mathrm{ST}}$	Proportional gain for knee joint during stance for leg k	4
	$K^k_{\mathrm{D},2\mathrm{ST}}$	Derivative gain for knee joint during stance for leg k	4
	$K^k_{\mathrm{P},3\mathrm{SW}}$	Proportional gain for ankle joint during swing for leg k	4
	$K^k_{\mathrm{D},3\mathrm{SW}}$	Derivative gain for ankle joint during swing for leg k	4
	$K^k_{\mathrm{P},3\mathrm{ST}}$	Proportional gain for ankle joint during stance for leg k	4
	$K^k_{\mathrm{D},3\mathrm{ST}}$	Derivative gain for ankle joint during stance for leg k	4
V	T	Stride time. Only for φ_{S} (Speed Maximization)	1 (ϕ_S)

https://doi.org/10.1017/S0263574719001413 Published online by Cambridge University Press

Table AVI. The optimal pose (P_a^k) and variables.

	Minimum torque					Maximum speed
Parameter	**0.10 m/s**	**0.50 m/s**	**1.00 m/s**	**1.50 m/s**	**1.97 m/s**	**1.97 m/s**
$\psi_{\text{net}}^{\text{FL}}$	0.289	0.585	0.559	0.202	0.391	0.172
$\dot{\psi}_{\text{AEP}}^{\text{FL}}$	−0.316	−0.187	0.013	−0.353	0.274	−0.110
$\dot{\psi}_{\text{PEP}}^{\text{FL}}$	−0.294	0.084	−0.146	−0.438	0.689	0.138
$\psi_{\text{net}}^{\text{FR}}$	0.711	0.477	0.344	0.707	0.437	0.659
$\dot{\psi}_{\text{AEP}}^{\text{FR}}$	0.035	0.025	−0.413	−0.263	0.219	−0.255
$\dot{\psi}_{\text{PEP}}^{\text{FR}}$	−0.259	0.063	−0.316	0.174	−0.317	−0.547
$\psi_{\text{net}}^{\text{HL}}$	0.488	0.795	0.800	0.799	0.800	0.791
$\dot{\psi}_{\text{AEP}}^{\text{HL}}$	−0.552	−0.612	0.068	−0.222	0.166	0.137
$\dot{\psi}_{\text{PEP}}^{\text{HL}}$	−0.156	−0.473	−0.259	−0.461	−0.128	0.068
$\psi_{\text{net}}^{\text{HR}}$	0.613	0.775	0.752	0.799	0.796	0.800
$\dot{\psi}_{\text{AEP}}^{\text{HR}}$	−0.215	−0.285	0.399	0.176	−0.293	0.089
$\dot{\psi}_{\text{PEP}}^{\text{HR}}$	−0.115	−0.434	−0.681	−0.700	−0.613	−0.700
$z_{\text{net}}^{\text{FL}}$	−0.000	−0.004	0.000	0.001	0.003	0.006
$z_{\text{net}}^{\text{FR}}$	−0.002	−0.000	−0.000	−0.002	−0.002	−0.000
$z_{\text{net}}^{\text{HL}}$	0.000	0.005	0.007	0.005	−0.010	0.002
$z_{\text{net}}^{\text{HR}}$	0.001	0.004	0.001	0.002	−0.005	−0.003
f_c^{FL}	0.035	0.053	0.045	0.024	0.076	0.070
f_c^{FR}	0.058	0.072	0.064	0.051	0.027	0.039
f_c^{HL}	0.058	0.014	0.030	0.038	0.027	0.040
f_c^{HR}	0.054	0.031	0.063	0.013	0.100	0.075

Table AVII. The optimal pose (P_b^k) variables.

	Minimum torque					Maximum speed
Parameter	**0.10 m/s**	**0.50 m/s**	**1.00 m/s**	**1.50 m/s**	**1.97 m/s**	**1.97 m/s**
$\theta_{1\ \text{AEP}}^{\text{FL}}$	−1.562	−1.567	−1.569	−1.565	−1.559	−1.549
$\theta_{2\ \text{AEP}}^{\text{FL}}$	0.892	0.883	0.903	0.910	0.937	0.898
$\theta_{3\ \text{AEP}}^{\text{FL}}$	−0.212	−0.239	−0.407	−0.37	−0.431	−0.461
$\theta_{1\ \text{AEP}}^{\text{FR}}$	−1.562	−1.645	−1.573	−1.547	−1.557	−1.572
$\theta_{2\ \text{AEP}}^{\text{FR}}$	0.894	0.890	0.902	0.892	0.892	0.912
$\theta_{3\ \text{AEP}}^{\text{FR}}$	−0.214	−0.162	−0.384	−0.349	−0.229	−0.403
$\theta_{1\ \text{AEP}}^{\text{HL}}$	−1.172	−1.124	−1.045	−0.802	−0.940	−1.031
$\theta_{2\ \text{AEP}}^{\text{HL}}$	−1.267	−1.037	−1.114	−1.207	−1.257	−1.186
$\theta_{3\ \text{AEP}}^{\text{HL}}$	1.277	1.338	1.322	1.003	1.297	1.312
$\theta_{1\ \text{AEP}}^{\text{HR}}$	−1.157	−1.118	−0.974	−0.923	−0.826	−0.950
$\theta_{2\ \text{AEP}}^{\text{HR}}$	−1.261	−1.147	−1.129	−1.225	−1.026	−1.167
$\theta_{3\ \text{AEP}}^{\text{HR}}$	1.274	1.288	1.192	1.199	0.999	1.172

https://doi.org/10.1017/S0263574719001413 Published online by Cambridge University Press

Table AVIII. The optimal pose (P_c) variables and stride time (T) for speed optimization.

	Minimum torque					Maximum speed
Parameter	**0.10 m/s**	**0.50 m/s**	**1.00 m/s**	**1.50 m/s**	**1.97 m/s**	**1.97 m/s**
λ	0.183	0.295	0.400	0.503	0.564	0.436
ψ_B	−0.005	−0.019	−0.007	−0.017	−0.047	−0.016
$\dot{y}_{B,i}$	0.002	0.038	0.043	0.048	0.043	0.046
T	–	–	–	–	–	0.227

Table AIX. The optimal gait variables.

	Minimum torque					Maximum speed
Parameter	**0.10 m/s**	**0.50 m/s**	**1.00 m/s**	**1.50 m/s**	**1.97 m/s**	**1.97 m/s**
ϕ^{FR}	0.491	0.469	0.453	0.454	0.549	0.540
ϕ^{HL}	0.633	0.666	0.734	0.733	0.599	0.720
ϕ^{HR}	0.239	0.242	0.218	0.217	0.220	0.220
β^{FL}	0.818	0.651	0.503	0.410	0.433	0.465
β^{FR}	0.805	0.679	0.500	0.416	0.330	0.484
β^{HL}	0.889	0.662	0.514	0.499	0.402	0.535
β^{HR}	0.855	0.585	0.501	0.426	0.413	0.529

Table AX. The optimal control variables for the front legs.

	Minimum torque					Maximum speed
Parameter	**0.10 m/s**	**0.50 m/s**	**1.00 m/s**	**1.50 m/s**	**1.97 m/s**	**1.97 m/s**
$K^{FL}_{P,1_{ST}}$	787.0	169.5	102.5	100.0	102.1	134.7
$K^{FL}_{D,1_{ST}}$	19.80	5.136	3.278	1.933	1.409	1.694
$K^{FL}_{P,2_{ST}}$	609.9	778.3	827.1	883.4	835.6	899.2
$K^{FL}_{D,2_{ST}}$	14.96	6.953	16.10	13.66	8.004	14.82
$K^{FL}_{P,3_{ST}}$	227.4	101.4	100.0	249.3	315.8	183.2
$K^{FL}_{D,3_{ST}}$	13.37	19.15	17.38	18.37	19.48	19.31
$K^{FL}_{P,1_{SW}}$	914.8	574.8	151.2	100.0	100.0	100.0
$K^{FL}_{D,1_{SW}}$	9.234	5.88	6.665	3.126	1.702	3.001
$K^{FL}_{P,2_{SW}}$	649.0	762.5	501.3	551.9	646.1	546.7
$K^{FL}_{D,2_{SW}}$	10.41	8.201	15.44	13.08	17.73	18.49
$K^{FL}_{P,3_{SW}}$	371.6	297.4	315.6	617.1	475.4	275.2
$K^{FL}_{D,3_{SW}}$	3.403	7.382	12.04	13.79	2.597	6.572
$K^{FR}_{P,1_{ST}}$	141.3	237.0	225.9	100.0	100.0	285.6
$K^{FR}_{D,1_{ST}}$	13.95	4.440	3.407	3.271	1.005	6.363
$K^{FR}_{P,2_{ST}}$	518.1	470.0	686.4	797.8	438.0	639.2
$K^{FR}_{D,2_{ST}}$	7.231	13.10	17.70	14.92	16.36	16.60
$K^{FR}_{P,3_{ST}}$	182.2	214.4	118.1	346.5	326.8	208.0
$K^{FR}_{D,3_{ST}}$	13.89	17.21	5.175	10.41	10.43	1.115
$K^{FR}_{P,1_{SW}}$	461.7	277.0	211.4	100.0	100.1	413.7
$K^{FR}_{D,1_{SW}}$	7.099	3.047	6.264	1.317	1.221	8.715
$K^{FR}_{P,2_{SW}}$	453.1	683.6	568.7	576.7	489.7	348.6
$K^{FR}_{D,2_{SW}}$	13.24	18.19	11.70	12.11	16.85	13.89
$K^{FR}_{P,3_{SW}}$	363.7	539.7	287.9	483.7	487.6	288.2
$K^{FR}_{D,3_{SW}}$	3.940	11.62	8.710	7.939	9.694	7.867

https://doi.org/10.1017/S0263574719001413 Published online by Cambridge University Press

Table AXI. The optimal control variables for the hind legs.

	Minimum torque					Maximum speed
Parameter	**0.10 m/s**	**0.50 m/s**	**1.00 m/s**	**1.50 m/s**	**1.97 m/s**	**1.97 m/s**
$K^{HL}_{P,1ST}$	128.8	100.2	100.0	100.1	100.2	122.3
$K^{HL}_{D,1ST}$	12.34	2.959	1.000	1.000	1.037	2.364
$K^{HL}_{P,2ST}$	821.0	524.1	479.3	814.5	668.0	578.1
$K^{HL}_{D,2ST}$	14.82	11.27	13.12	11.42	16.01	14.04
$K^{HL}_{P,3ST}$	323.1	520.9	248.2	239.7	345.2	314.9
$K^{HL}_{D,3ST}$	12.03	11.56	15.39	14.77	19.34	17.72
$K^{HL}_{P,1SW}$	722.0	279.6	100.4	103.6	100.0	127.6
$K^{HL}_{D,1SW}$	3.174	6.041	1.659	1.000	1.639	1.175
$K^{HL}_{P,2SW}$	491.3	431.2	902.1	720.3	573.6	769.6
$K^{HL}_{D,2SW}$	1.285	6.331	1.000	1.827	1.98	1.844
$K^{HL}_{P,3SW}$	464.9	546.6	799.8	744.9	652.3	736.1
$K^{HL}_{D,3SW}$	12.60	12.26	16.87	12.26	19.49	18.08
$K^{HR}_{P,1ST}$	101.3	100.0	100.0	100.0	133.5	114.7
$K^{HR}_{D,1ST}$	9.792	1.000	1.000	1.000	1.068	2.947
$K^{HR}_{P,2ST}$	518.9	861.2	536.0	225.1	428.5	582.3
$K^{HR}_{D,2ST}$	16.63	12.96	17.05	16.62	18.37	19.46
$K^{HR}_{P,3ST}$	347.4	280.5	608.5	603.0	430.4	293.5
$K^{HR}_{D,3ST}$	11.30	18.39	15.67	13.69	17.80	19.49
$K^{HR}_{P,1SW}$	788.7	248.8	102.3	132.2	141.7	163.6
$K^{HR}_{D,1SW}$	1.000	3.650	2.153	2.587	1.251	1.000
$K^{HR}_{P,2SW}$	556.3	800.0	499.1	524.5	403.1	535.5
$K^{HR}_{D,2SW}$	6.304	5.925	8.914	8.450	10.26	7.779
$K^{HR}_{P,3SW}$	508.3	764.9	149.0	250.4	104.2	264.1
$K^{HR}_{D,3SW}$	9.772	13.77	8.694	8.144	14.03	10.79

https://doi.org/10.1017/S0263574719001413 Published online by Cambridge University Press